2.05 Mineralogy of the Deep Mantle – The Post-Perovskite Phase and its Geophysical Significance

K Hirose, Tokyo Institute of Technology, Tokyo, Japan
R Wentzcovitch and DA Yuen, University of Minnesota, Minneapolis, MN, USA
T Lay, University of California Santa Cruz, Santa Cruz, CA, USA

Glossary

CMB The core–mantle boundary is the surface defined by the contrast in composition between silicate and oxide crystalline rocks in the mantle and molten iron alloy in the core.

D″ Designation for the lowermost 200–300 km of the lower mantle. This region is distinct from the overlaying mantle in that the seismic velocity variations are not consistent with homogeneous material under self-compression and an adiabatic temperature gradient.

DAC Diamond-anvil cell compression devices in which a sample is compressed between faceted diamonds, often with laser heating, to achieve high *P*–*T* conditions such as in the lower mantle and core.

2.05.1 Lower Mantle Mineralogy

The Earth's uppermost mantle is peridotitic (pyrolytic) in composition based on petrologic evidence (McDonough and Sun, 1995). Given that the global seismic velocity discontinuity observed at 410 km depth can be reconciled with a phase transition from olivine to wadsleyite, the transition zone should also be peridotitic in composition, although it could be contaminated by subducted former oceanic lithosphere with an ecologitic component (e.g., Irifune et al., 2008; Nishihara et al., 2005). On the other hand, the chemical composition of the lower mantle is a matter of ongoing debate. It is generally believed that the bulk Earth composition is similar to solar abundance or the nonvolatile element composition of primitive meteorites (CI chondrites). If this is the case, the Mg/Si ratio of the Earth's mantle should be close to 1.0, while the peridotitic upper mantle shows Mg/Si = 1.27, with Mg_2SiO_4 olivine as the most abundant mineral. In order to reconcile the chondritic Earth model with the peridotitic mantle, Allègre et al. (1995) proposed 5 wt% Si in the core as its primary light alloy component. Alternatively, the lower mantle could be Si-enriched relative to the upper mantle and composed primarily of $MgSiO_3$-rich perovskite.

Recent experimental and geophysical modeling studies have supported a perovskititic lower mantle. Ricolleau et al. (2009) argued that the Preliminary Reference Earth Model (PREM)

density profile of the lower mantle is compatible with single-phase perovskite, on the basis of *P*–*V*–*T* (pressure–volume–temperature) equation of state (EoS) of $MgSiO_3$-rich perovskite formed in a natural peridotite bulk composition. However, the chemical composition of $MgSiO_3$-rich perovskite may have changed with changing *P*–*T* conditions during their measurements because it coexisted with (Mg,Fe)O ferropericlase in the sample. More recently, Murakami et al. (2012) measured shear-wave velocities of $MgSiO_3$ perovskite and MgO to 91 GPa and 2700 K and also estimated the effects of Al and Fe impurities for room-temperature measurements to 124 GPa. Comparing the velocities of (Fe,Al)-bearing $MgSiO_3$ perovskite and (Mg,Fe)O ferropericlase to the PREM velocity profile, Murakami et al. concluded that the lower mantle is composed of more than 93% $MgSiO_3$-rich perovskite, consistent with a chondritic lower mantle model rather than a peridotitic mantle model. First-principles studies spanning two decades not only support a peridotitic uppermost lower mantle but also suggest that PREM (Dziewonski and Anderson, 1981) velocities deviate from a peridotitic composition in the deeper lower mantle (da Silva et al., 2000; Karki et al., 2001; Wentzcovitch et al., 2004, 2009; Zhang et al., 2014). Part of the deviation is likely to be related with the post-perovskite transition (Wentzcovitch et al., 2004). Thermodynamic modeling also suggests deviations from a peridotitic mantle (Xu et al., 2008), while a more recent first-principles molecular dynamics (MD) gives additional support to a peridotitic lower mantle (Zhang et al., 2014).

Regardless of this evolving mineral physics perspective, it is widely believed that the whole mantle is being mixed and the lower mantle is thus commonly inferred to be similar in composition to the peridotitic upper mantle. The experiments by Irifune et al. (2010) using multianvil apparatus with sintered diamond anvils showed phase assemblage and proportion in a peridotitic lower mantle to 47 GPa and 2073 K to be 74 vol.% $MgSiO_3$-rich perovskite, 18 vol.% ferropericlase, and 8 vol.% $CaSiO_3$ perovskite. Kesson et al. (1998) demonstrated through a combination of diamond anvil cell (DAC) experiments and chemical analysis using transmission electron microscope (TEM) that a peridotitic deep lower mantle should consist of 69 wt% $MgSiO_3$-rich perovskite, 22 wt% ferropericlase, and 9 vol.% $CaSiO_3$ perovskite. With similar techniques, Murakami et al. (2005) reported 72 vol.% post-perovskite, 21 wt% ferropericlase, and 7 wt% $CaSiO_3$ perovskite for *P*–*T* conditions in the lowermost mantle. Trampert et al. (2004) found, however, that the proportion of $MgSiO_3$-rich perovskite is variable by up to ±10% in the lower mantle. The lower mantle is probably primarily (69–93 wt%) $MgSiO_3$-rich perovskite, so the stability and property of this phase have been extensively studied.

2.05.2 Post-Perovskite Phase

2.05.2.1 Discovery

Silicate perovskite was first synthesized at 30 GPa based on laser-heated DAC technique by Liu (1974). Since then, $MgSiO_3$-rich perovskite is known to be a primary constituent in the lower mantle, consisting about 70% of a peridotitic lower mantle as noted earlier in the text, coexisting with minor amounts of (Mg,Fe)O ferropericlase and $CaSiO_3$ perovskite (Hirose, 2002; Irifune, 1994; Wood, 2000). While seismology has shown that the lowermost few hundred kilometers of the mantle, called the D″ layer, has distinct properties and a widespread seismic velocity discontinuity (Lay and Helmberger, 1983), it was initially believed that $MgSiO_3$-rich perovskite is stable down to the core–mantle boundary (CMB). Indeed, Knittle and Jeanloz (1987) reported the stability of orthorhombic $(Mg,Fe)SiO_3$ perovskite up to 127 GPa, close to the D″ conditions. Subsequent experimental and theoretical studies supported the stability of $MgSiO_3$-rich perovskite into the deep lower mantle (e.g., Andrault, 2001; Fiquet et al., 2000; Karki et al., 2000; Kesson et al., 1998; Wentzcovitch et al., 1993). Some form of solid–solid phase transition with a positive Clapeyron slope in the lowermost mantle was suggested from the correlation between temperature-modulated velocity anomalies and elevation of the observed D″ S-wave velocity discontinuity, but this was speculative (Sidorin et al., 1999).

Conventionally, the identification of a high-pressure phase is made after the sample is recovered at ambient conditions. In the early 1990s, intense synchrotron x-rays became available to examine crystal structure *in situ* at high *P*–*T* (see a review by Yagi, 2007). Such *in situ* experiments are important in particular for metals because high-pressure forms of metal usually transform back to low-pressure forms during decompression. This is sometimes true for silicates as well. Indeed, $MgSiO_3$ post-perovskite cannot be quenched to ambient conditions as it converts to amorphous structure upon decompression; therefore, *in situ* observations were key to its discovery.

Murakami et al. performed x-ray diffraction (XRD) measurements *in situ* for the lowermost mantle *P*–*T* conditions, based on a combination of laser-heated DAC and synchrotron radiation at SPring-8. In 2002, they first observed a number of unknown diffraction peaks in the XRD patterns of natural peridotite composition at pressures higher than 120 GPa (Murakami et al., 2005). Subsequently, they analyzed $MgSiO_3$ and found similar radical changes in the XRD patterns when $MgSiO_3$ perovskite was heated to 2500 K at 127 GPa (**Figure 1(a)** and **1(b)**) (Murakami et al., 2004). Importantly, such conversion was found to be reversible; the pattern changed back to that of perovskite when the sample was decompressed and reheated at 89 GPa (**Figure 1(c)**). These observations indicated a phase transition from $MgSiO_3$ perovskite to a new polymorph, now called post-perovskite.

The crystal structure of $MgSiO_3$ post-perovskite was determined with the aid of computational MD simulations (Murakami et al., 2004). The details of structure determination by MD calculations were reported in Hirose and Kawamura (2007). 'Perovskite' has a family of related structures with a vast range of chemical compositions. Nevertheless, the XRD peaks observed by Murakami et al. are not accounted for with any perovskite-type structure. Pressure-induced phase transformations from perovskite to denser structures were not known at that time. Tsuchiya et al. (2004b) independently obtained this structure using first-principles MD simulations with variable cell shape (Wentzcovitch et al., 1993) guided by a rationale based on pressure-induced structural distortion of perovskite (Wentzcovitch et al., 1995). The search was motivated by the XRD data of Murakami et al. (2004), which, together with thermodynamic stability calculations (Tsuchiya et al., 2005a), confirmed the nature of the identified structure

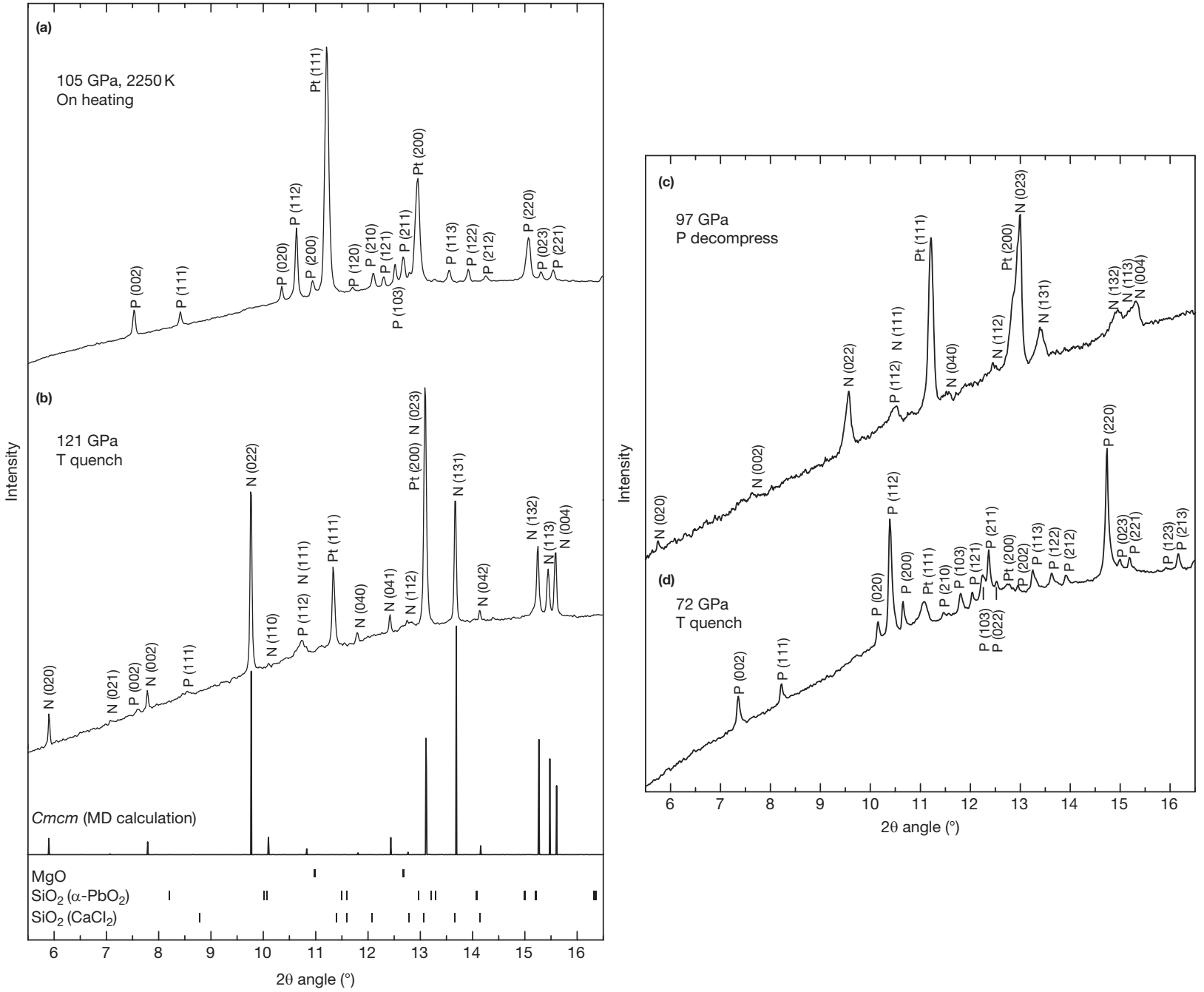

Figure 1 XRD patterns of $MgSiO_3$. (a) Perovskite at 105 GPa and 2250 K, (b) post-perovskite at 121 GPa and 300 K after heating at 127 GPa, (c) post-perovskite at 97 GPa and 300 K after decompression from 125 GPa, and (d) perovskite at 72 GPa and 300 K after heating at 89 GPa (after Murakami et al., 2004). P, perovskite; Pt, platinum; N, new phase (post-perovskite). In (b), the calculated powder XRD pattern of post-perovskite (space group: *Cmcm*) and the peak positions of MgO and SiO_2 (both α-PbO_2-type and $CaCl_2$-type structures) are shown.

at experimental conditions. The crystal structure of post-perovskite and the envisioned relationship between the perovskite and post-perovskite structures are illustrated in **Figure 2**. The coordination numbers of Si and Mg remain six and eight, respectively, as in perovskite. The Mg^{2+} site in post-perovskite is smaller than in perovskite, which results in a volume reduction of 1.0–1.5% (Iitaka et al., 2004; Tsuchiya et al., 2004b). Oganov and Ono (2004) also obtained the same structure from the analogy of similar phase transition in Fe_2O_3. This structure is the same as those of $UFeS_3$ (Noel and Padiou, 1976) and $CaIrO_3$ (McDaniel and Schneider, 1972), both of which are stable at ambient pressure.

2.05.2.2 Stability

Post-perovskite-type phase transitions have now been reported in a variety of simple and multicomponent systems: $MgSiO_3$ (Hirose et al., 2006a; Murakami et al., 2004; Oganov and Ono, 2004; Ono and Oganov, 2005; Shim et al., 2004; Tsuchiya et al., 2004a,b), $MgGeO_3$ (Hirose et al., 2005b), $MnGeO_3$ (Tateno et al., 2006), $ZnGeO_3$ (Yusa et al., 2005), $CaIrO_3$ (Hirose and Fujita, 2005; Kojitani et al., 2007), Al_2O_3 (Akber-Knutson et al., 2005; Caracas and Cohen, 2005; Oganov and Ono, 2005; Stackhouse et al., 2005a,b; Tsuchiya et al., 2005b), Fe_2O_3 (Ono and Ohishi, 2005; Ono et al., 2004), Mn_2O_3 (Santillán et al., 2006), $NaMgF_3$ (Martin et al., 2006; Umemoto et al., 2006a), and natural pyrolite (KLB-1 peridotite) (Grocholski et al., 2012; Murakami et al., 2005; Ohta et al., 2008a; Ono and Oganov, 2005), normal mid-ocean ridge basalt (MORB) compositions (Grocholski et al., 2012; Hirose et al., 2005a; Ohta et al., 2008a; Ono et al., 2005), harzburgite composition (Grocholski et al., 2012), and San Carlos olivine (Grocholski et al., 2012). $CaIrO_3$ has been often used as an analog of $MgSiO_3$ post-perovskite to explore

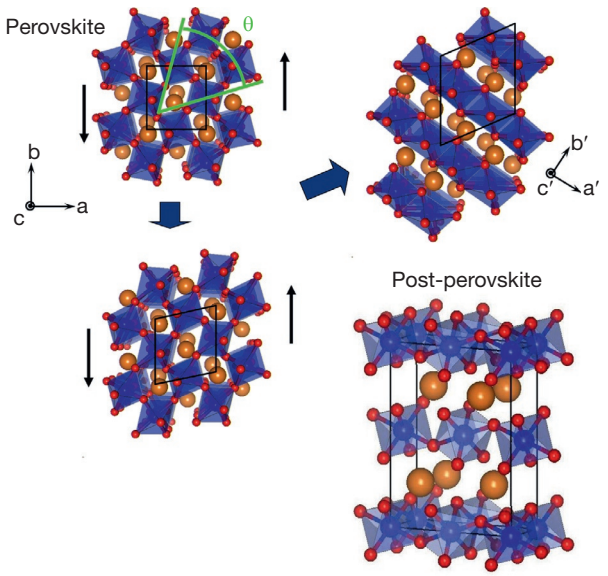

Figure 2 Structural relation between perovskite and post-perovskite under a shear deformation ε_6 (Tsuchiya et al., 2004a,b). This relationship corresponds to the distortion associated with a nucleation center of the post-perovskite transition (Oganov et al., 2005).

the Clapeyron slope of the perovskite/post-perovskite phase transition boundary (Hirose and Fujita, 2005; Kojitani et al., 2007), compression behavior (e.g., Martin et al., 2006), deformation mechanism (e.g., Walte et al., 2007, 2009), rheology (Hunt et al., 2009), grain growth (Yoshino and Yamazaki, 2007), etc., which are difficult to experimentally examine *in situ* for the lowermost mantle high *P*–*T* conditions.

2.05.2.2.1 Post-perovskite phase boundary in pure $MgSiO_3$

The determination of the thermodynamic post-perovskite boundary in $MgSiO_3$ post-perovskite is important to shed light on the nature of the D″ region. This is a challenging task for both experiments and computations for several reasons. *In situ* crystallography based on DAC has been extended to the multi-Mbar regime, and temperatures in these experiments have crossed the 6000 K mark. However, high *P*–*T* calibration standards still give uncertainties about the post-perovskite phase boundary. Computations based on density functional theory (DFT) (Hohenberg and Kohn, 1964; Kohn and Sham, 1965) suffer from uncertainties related with the choice of the approximation used to describe the exchange–correlation energy of electrons and of the approach used to describe ionic motion: quantum at relatively low temperatures or classical at relatively high temperatures.

The first report on $MgSiO_3$ post-perovskite by Murakami et al. (2004) found that it exists above 125 GPa and 2500 K, but did not tightly constrain the *P*–*T* location of the boundary. Later, Tateno et al. (2009) demonstrated on the basis of experiments to 171 GPa and 4400 K that the phase transition boundary between perovskite and post-perovskite in pure $MgSiO_3$ is located at 121 GPa corresponding to 2650 km depth at a plausible deep lower mantle temperature of 2400 K (**Figure 3**).

Recently, the accuracy of the pressure scale used to determine experimental pressure has been a matter of extensive debate (e.g., Fei et al., 2004; Hirose, 2007). With synchrotron XRD measurements, pressure at high temperature is calculated from the *P*–*V*–*T* EoS of an internal pressure standard loaded together with a sample. The typical pressure standards include Au, Pt, MgO, and NaCl. However, it is known that each standard indicates a different pressure, sometimes with differences of more than 10 GPa at ~120 GPa even at room temperature (Akahama et al., 2002; Hirose et al., 2008a; Matsui et al., 2009). Even using a given pressure standard, different EoSs show different pressures; for example, the EoS of Au proposed by Fei et al. (2007) gives pressure higher by about 12 GPa at 110 GPa/2400 K than that reported by Anderson et al. (1989) (Hirose et al., 2008a). On the other hand, Fei et al. (2007) proposed internally consistent pressure scales (EoSs) of Au, Pt, NaCl, and Ne primarily based on the MgO scale reported by Speziale et al. (2001). Similar efforts to establish consistent pressure scales are also found in Dorogokupets and Dewaele (2007).

The post-perovskite phase transition boundary in pure $MgSiO_3$ has been experimentally determined using different pressure standards of Pt, Au, and MgO (Hirose et al., 2006a; Ono and Oganov, 2005; Tateno et al., 2009) (**Figure 3**). These results reported transition pressures differing by more than 15 GPa, but this inconsistency can be explained by the difference in pressure scales. Ono and Oganov (2005) demonstrated that the transition occurred above 130 GPa and 2500 K based on the Pt scale proposed by Holmes et al. (1989). Such

relatively high transition pressure is consistent with the earlier observation that the Pt scale predicts much higher pressure than the Au scale in this pressure range at 300 K (Akahama et al., 2002). On the other hand, Hirose et al. (2006a) demonstrated that the transition boundary is located at much lower pressure, 113 ± 2 GPa at 2400 K, when using the Au scale proposed by Tsuchiya (2003). Note that the Tsuchiya (2003) Au EoS predicts lower pressure by 6 GPa than the MgO scale (Hirose et al., 2008a), which accounts for discrepancy with the results by Tateno et al. (2009) using the MgO scale.

As far as computations are concerned, the basic theoretical framework for these calculations, DFT, is in principle exact. However, this is a one-electron approach and, in practice, approximations for the electronic exchange–correlation energy

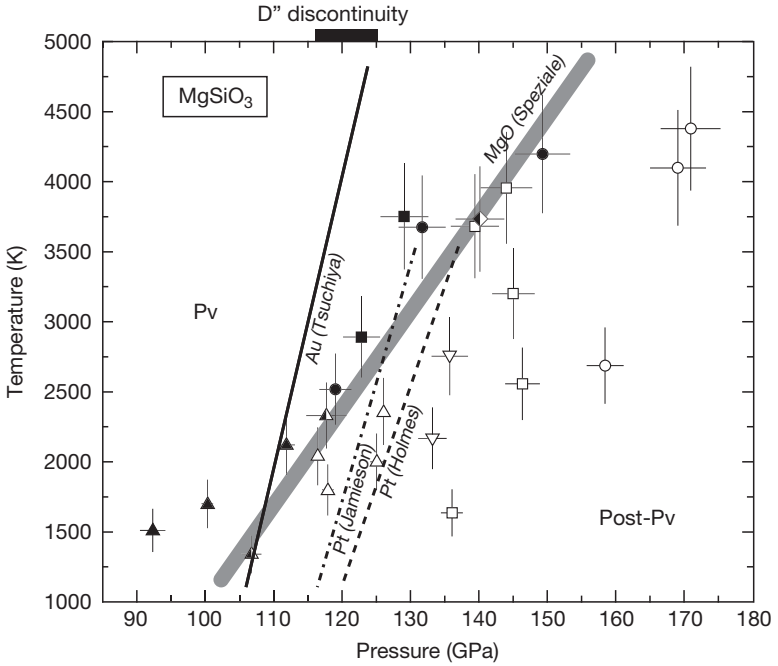

Figure 3 Post-perovskite phase transition boundary in $MgSiO_3$ determined by high-pressure experiments (Tateno et al., 2009) based on MgO pressure scale (Speziale et al., 2001). Other experimental results by Hirose et al. (2006), Murakami et al. (2004), and Ono and Oganov (2005) are also shown, which used Au scale proposed by Tsuchiya (2003), Pt scales by Jamieson et al. (1982) and Holmes et al. (1989), respectively.

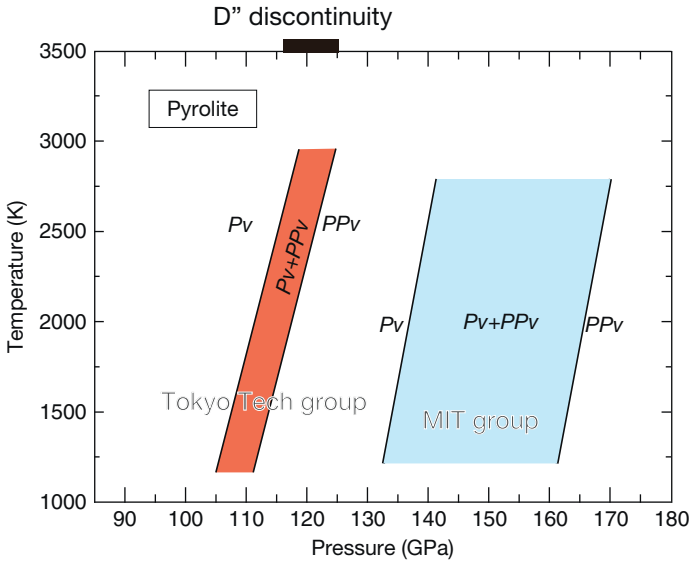

Figure 4 Post-perovskite phase transition boundary in a natural pyrolitic mantle determined by Tokyo Tech group (Murakami et al., 2005; Ohta et al., 2008a) (orange) and by MIT group (Grocholski et al., 2012) (blue). The former studies showed that the transition pressure matches the depth of the D″ discontinuity, but the latter reported much higher transition pressure.

must be made. Among these, the local-density approximation (LDA) (Perdew and Zunger, 1981) and the generalized gradient approximations (GGAs) (Perdew et al., 1996) are the most popular and best tested. The second issue is the computation of free energy associated with atomic motion – quantum at low and classical at high temperatures. Two distinct approximations exist for these limits: The quasi-harmonic approximation (QHA) for low-temperature calculations (Wallace, 1972) assumes atomic vibrations are harmonic, the harmonic potential is only volume-dependent, and vibrational modes do not interact. This approximation proved to be extremely good for several mantle minerals, including $MgSiO_3$ perovskite and post-perovskite (Wentzcovitch et al., 2010). However, vibrations can be quite anharmonic at high temperatures near melting and atomic motion is essentially classical. In this limit, the method of choice is MD with one caveat – the number of atoms used in simulations needs to be large, $\sim 10^4$, for converged free energy results (Belonoshko et al., 2005). This is in practice beyond the capability of DFT-based calculations and MD with considerably smaller number of atoms is the norm (e.g., Oganov et al., 2001; Zhang et al., 2013). Near phase transitions, anharmonicity may also be very important and quantum in nature. This can complicate greatly the calculation and strategies are still being sought for this case (Zhang et al., 2013). Fortunately, at relevant conditions, $MgSiO_3$ perovskite and post-perovskite seem to lie well within the range of validity of the QHA (Carrier et al., 2007; Tsuchiya et al., 2005a). Therefore, the QHA has been used in conjunction with vibrational frequencies calculated using density functional perturbation theory to compute free energies of perovskite and post-perovskite. The resulting phase boundary is displayed in Figure 5. The calculated Clapeyron slope of this transition, 7.5 MPa K^{-1}, differs somewhat from measurements (see Table 1), and the deviation seems to be larger than the uncertainty caused by the use of different exchange–correlation functionals, that is, LDA (Perdew and Zunger, 1981) or GGA (Perdew et al., 1996). Anharmonic effects on this phase boundary may be important (Zhang et al., 2013) but have not been investigated yet. Although the phase boundary uncertainty is large, this transition is plausibly associated with the D″ discontinuity at ~125 GPa.

2.05.2.2.2 Post-perovskite phase boundary in peridotitic mantle

The post-perovskite phase transition has been observed not only in pure $MgSiO_3$ but also in natural compositions such as peridotitic mantle and MORB materials. Murakami et al. (2005) first reported the post-perovskite phase transition in 'pyrolite' (KLB-1 peridotite) above 113 GPa and 2500 K based on the Au scale by Tsuchiya (2003), which is recalculated to 120 GPa when using Speziale et al.'s (2001) MgO scale and thus similar to the transition pressure in pure $MgSiO_3$ (Figure 4). Following up their experiments, Ohta et al. (2008a) augmented the data and demonstrated that the transition occurs between 116 and 121 GPa at 2500 K using the Au scale by Hirose et al. (2008a) that was made on the basis of the Speziale et al.'s MgO scale.

Ono and Oganov (2005) performed similar XRD measurements to determine the phase transition boundary in KLB-1 peridotite. Their results showed that the transition took place at 124 GPa and 2500 K based on the Au scale proposed by Jamieson et al. (1982), which is equivalent to 134 GPa if we use Speziale et al.'s MgO scale. Furthermore, recent experiments by Grocholski et al. (2012) reported the transition as between 140 and 169 GPa at 2500 K by Tsuchiya's (2003) Au scale, (Figure 4) which is converted into 146 and 175 GPa using the MgO scale.

These indicate that the post-perovskite transition pressure estimates in natural peridotite compositions determined by earlier DAC experiments differ by more than 20 GPa (Figure 4). Indeed, the pressure range of the phase transition in a natural peridotite composition (140–169 GPa) reported by Grocholski et al. (2012) is much higher than 112–140 GPa in $(Mg_{0.9}Fe_{0.1})(Al_{0.1}Si_{0.9})O_3$ determined by the same group

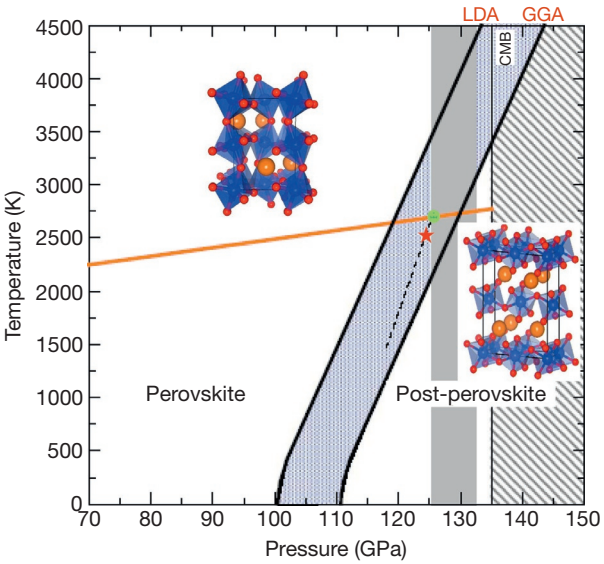

Figure 5 Post-perovskite phase boundary calculated using the local-density approximation (LDA) and generalized gradient approximation. The width of the stripe displays the typical uncertainty associated with the approximations to exchange–correlations energy of the electrons (from Tsuchiya et al., 2004a). The dashed line is the phase boundary proposed by combining experimental transition data (red star) (Murakami et al., 2004) and the Clapeyron slope used to explain the D″ topography by a solid–solid phase change (Sidorin et al., 1999). The vertical gray bar corresponds to the pressure range across the D″ topography. The orange line corresponds to the mantle adiabat (Brown and Shankland, 1981).

Table 1 The Clapeyron slope of the $MgSiO_3$ post-perovskite phase transition

	Clapeyron slope (MPa K^{-1})	*Source*
Wu et al.'s scale (2008)	9.7	Hirose et al. (2006a)
Speziale et al.'s scale (2001)	11.5	Hirose et al. (2006a)
Tsuchiya (2004)	5.0	Hirose et al. (2006a)
Holmes et al.'s Pt scale (1989)	7.0	Ono and Oganov (2005)
Jamieson et al.'s Au scale (1982)	8.0	Ono and Oganov (2005)
Theory	7.5,[a] 9.85[b]	

[a]Tsuchiya et al. (2004a,b).
[b]Oganov and Ono (2004).

(Catalli et al., 2009). The main difference between the natural peridotite and $(Mg_{0.9}Fe_{0.1})(Al_{0.1}Si_{0.9})O_3$ bulk compositions is the presence of ferropericlase, which narrows the width (pressure range) of the transition but does not increase the average transition pressure (Sinmyo et al., 2011). The origin of inconsistency between Catalli et al. (2009) and Grocholski et al. (2012) is not clear.

One possible source of discrepancy between the previous experimental results is kinetic hindering of the post-perovskite phase transition. Ono and Oganov (2005) repeated a number of heating cycles with changing P–T condition for a given sample to evaluate the growth/reduction of diffraction peaks of perovskite and post-perovskite. However, the transition may have been kinetically hindered in their experiments because phase transitions are commonly sluggish after a high-pressure phase is formed in the first heating cycle (Hirose et al., 2006b). Grocholski et al. (2012) also heated a specific sample repeatedly with changing P–T conditions although the data obtained in the first heating cycle alone defined the relatively high-pressure condition of the phase transition.

Another source of discrepancy is thermal diffusion, often called Soret diffusion, during laser heating. The temperature gradient in a laser-heated sample is relatively large, typically ±10%, such that iron migrates to the low-temperature part of the sample (Sinmyo and Hirose, 2010). The long heating duration in laser-heated DAC experiments does not necessarily attain chemical equilibrium (sample grain size is usually limited only to 100 nm and thus long heating duration is not required for equilibrium) but often causes depletion in iron at the hot spot in particular when the sample is mixed with a metal powder of laser absorber (Sinmyo and Hirose, 2010).

Discrepancies in predicted post-perovskite phase transition characteristics are found not only in the average transition pressure but also in the pressure interval of the phase transition (pressure range for coexistence of perovskite and post-perovskite). Experiments by Ono and Oganov (2005) showed a pressure width of less than 3 GPa, corresponding to <50 km depth interval in the deep mantle. Ohta et al. (2008a) demonstrated a pressure width of 5 GPa that corresponds to a depth interval of 90 km. These are slightly broader but generally consistent with the possible sharpness of the D″ discontinuity; seismology has inferred a depth extent of velocity increase up to 50–75 km (Lay, 2008; Revenaugh and Jordan, 1991; Weber et al., 1996) or less than 30 km (Lay and Young, 1989). Note that prediction of too wide of a two-phase domain may in part be due to the errors in pressure determinations in the experiments. On the other hand, a similar discrepancy between seismic observations and experiments has been found for the 410 km seismic discontinuity. The effective depth extent of the seismological expression of the olivine to β-spinel transition may be less than half of the two-phase coexistence region (Stixrude, 1997); possibly, this is also true for the post-perovskite phase transition.

More problematic is the Grocholski et al. (2012) estimation that the post-perovskite transition occurred over a pressure interval of about 25 GPa, much broader than observed by Ono and Oganov (2005) and Ohta et al. (2008a), and incompatible with the existence of a broadband seismic reflecting boundary. Previously, Catalli et al. (2009) and Andrault et al. (2010) also found that the width of the perovskite–post-perovskite two-phase coexistence region is larger than 20 GPa in Al-bearing $(Mg,Fe)SiO_3$ bulk composition. Nevertheless, Sinmyo et al. (2011) argued that the iron content in post-perovskite reduces from that of perovskite in the presence of (Mg,Fe)O ferropericlase, which acts to sharpen the transition. As a result, Grocholski et al. (2012) suggested that Al is key for both deepening and broadening the post-perovskite phase transition, but previous experiments and calculations showed that the effect of 4 wt% Al_2O_3 is not large enough to explain the results of Grocholski et al. (2012) (Akber-Knutson et al., 2005; Tateno et al., 2005; Tsuchiya and Tsuchiya, 2008). The XRD patterns by Grocholski et al. (2012) include peaks from nitrogen, which was possibly contaminated during cryogenic loading. This might be the source of the discrepancy although the effect of nitrogen is not known. If the phase transition is too gradual to produce a seismic reflection and only is manifested in a gradual velocity increase with depth, it is much harder to uniquely demonstrate the existence of post-perovskite phase in the mantle.

Surely, mantle mineralogy in the deep mantle is likely to be complex, and transition pressures and intervals can be quite sensitive to composition, mineralogy, temperature, etc. Thermodynamic equilibrium calculations in aggregates containing iron- and aluminum-bearing solid solutions, including strong electronic correlation, with spin crossover in ferric iron, and coexisting with ferropericlase, also undergoing spin crossover in ferrous iron, complicate tremendously the problem. Progress is steady though, but thermodynamic modeling needs to be aided by experimental data to give confidence in the calculations.

2.05.2.2.3 Compositional effects

Since the lowermost mantle is a mantle convection boundary layer, it is likely to be chemically heterogeneous due to the accumulation of dense materials. Such dense materials may include subducted MORB crust (Hirose et al., 2005a; Nakagawa and Tackley, 2005; Ricolleau et al., 2010), proto-crust formed and subducted in the early Earth (Boyet and Carlson, 2005; Tolstikhin and Hofmann, 2005), banded iron formation (Dobson and Brodholt, 2005), and products of late-stage crystallization from a basal magma ocean (Labrosse et al., 2007). Such chemical heterogeneity may produce seismic velocity structures including rapid velocity increases and decreases and large-scale lateral variations that make it difficult to identify any phase transition effects, particularly since chemical variations can affect the transition pressure and relative P- and S-wave velocity changes.

The post-perovskite phase transition has been experimentally observed for MORB materials. Combining with Hirose et al. (2005a), the experiments by Ohta et al. (2008a) reported that the transition occurred between 112 and 117 GPa at 2500 K using the Au pressure scale proposed by Hirose et al. (2008a), which was based on and therefore equivalent to the MgO scale. Similar experiments by Grocholski et al. (2012) also demonstrated that MORB underwent transition to post-perovskite between 108 and 122 GPa, broadly consistent with Ohta et al. (2008a). The transition pressure in MORB is lower than that in a peridotitic mantle by at least 4 GPa. It is also noted that MORB includes large amounts (~25%) of silica phase unlike peridotitic mantle material, and the silica phase undergoes structural transition from $CaCl_2$ type to α-PbO_2 structure in a similar pressure range (Grocholski et al., 2012; Hirose et al., 2005a), resulting in a shear-wave velocity decrease (Karki et al., 1997).

A seismologically observed shear-wave velocity reduction at 2530 km depth (Ohta et al., 2008a) and at 2550–2750 km depth (Konishi et al., 2009) has been attributed to these phase transitions occurring in chemically distinct mantle regions identified as large low shear velocity provinces (LLSVPs) that may have accumulated MORB material.

Detailed compositional effects on the post-perovskite phase transition have been extensively studied. All experimental and theoretical studies except Tsuchiya and Tsuchiya (2008) indicate that the addition of Al stabilizes perovskite at higher pressure relative to post-perovskite (Akber-Knutson et al., 2005; Caracas and Cohen, 2005; Tateno et al., 2005). Experiments by Tateno et al. (2005) showed that the transition starts at 140 GPa at 2500 K in $MgSiO_3 + 25$ mol% Al_2O_3 and the pressure interval of transition may be as large as 30 GPa. This suggests that ~5 mol% Al_2O_3 in both perovskite and post-perovskite in a pyrolytic lower mantle may increase the initiation of the post-perovskite phase transition by 3 GPa and the pressure interval by 6 GPa compared to pure $MgSiO_3$. The calculations by Akber-Knutson et al. (2005) also suggested that the transition occurs between 127 and 140 GPa at 2500 K in $MgSiO_3 + 6.25$ mol% Al_2O_3.

On the other hand, the effect of iron has been controversial. Experiments performed by Mao et al. (2004) demonstrated that the post-perovskite phase transition occurred in (Mg,Fe)SiO_3 around 110 GPa, which is much lower than the 125 GPa determined for pure $MgSiO_3$ by Murakami et al. (2004). More recently, Dorfman et al. (2012) showed that post-perovskite started to form in $(Mg_{0.61}Fe_{0.38}Ca_{0.01})SiO_3$ bulk composition at 87 GPa and 2150 K. These experimental results are supported by theory, which predicts that the post-perovskite structure is stable with respect to perovskite in $FeSiO_3$ end-member at all pressures in the Earth's mantle (e.g., Caracas and Cohen, 2005; Stackhouse et al., 2006). Contrary to these experimental and theoretical studies, Murakami et al. (2005) showed that Mg-perovskite is more iron-rich than post-perovskite in a natural pyrolite bulk composition, suggesting that iron stabilizes perovskite relative to post-perovskite. This is reinforced by the later phase transition study on (Mg,Fe)SiO_3 perovskite by Tateno et al. (2007) and the TEM studies by Hirose et al. (2008a,b) and Sinmyo et al. (2011).

2.05.2.2.4 Clapeyron slope of the phase transition boundary

The high positive Clapeyron slope of the post-perovskite phase transition was first estimated by theoretical calculations, although an unspecified solid–solid transition in the deep lower mantle with the slope of +6 MPa K^{-1} had been proposed to explain seismological detection of depth variations of the D″ discontinuity before the discovery of post-perovskite (Sidorin et al., 1999). Tsuchiya et al. (2004b) calculated the phase transition boundary at high temperatures, estimating a Clapeyron slope of +7.5 MPa K^{-1}. A slightly larger (about +10 MPa K^{-1}) slope was predicted by Oganov and Ono (2004).

High-pressure DAC experiments also indicate a large positive value of the Clapeyron slope for the post-perovskite phase transition in pure $MgSiO_3$, although the results are strongly dependent on the pressure scale. Ono and Oganov (2005) estimated +7 MPa K^{-1} based on the Holmes et al. (1989) Pt pressure scale. Hirose et al. (2006a) reported +5 MPa K^{-1} using Tsuchiya's Au scale and +11 MPa K^{-1} with Speziale et al.'s MgO scale. More recent study by Tateno et al. (2009) based on experiments over much wider P–T range gave +13 MPa K^{-1} based on the MgO scale. Similar high positive Clapeyron slope is also found in post-perovskite phase transition in analog material such as $CaIrO_3$ (+17 MPa K^{-1}) (Hirose and Fujita, 2005).

A special thermal EoS for MgO was engineered with accuracy of few GPa up to ~5000 K and 400 GPa to reinterpret data on the post-perovskite transition boundary (Wu et al., 2008). It combined consistently DAC data, ultrasound velocity data, and first-principles results. The experimental post-perovskite phase boundary obtained using this EoS gave a Clapeyron slope more consistent with those obtained by first-principles calculations (Oganov and Ono, 2004; Tsuchiya et al., 2004a,b) (see **Table 1**). It also supported the idea that the post-perovskite phase transforms back to perovskite in a high temperature gradient just above the CMB (Hernlund et al., 2005).

The determination of the Clapeyron slope for a natural mantle composition is more difficult than for pure $MgSiO_3$, because the transition (1) occurs over some pressure range and (2) is more sluggish in a multicomponent system. Experiments performed by Ohta et al. (2008a) did not tightly constrain but best estimated the Clapeyron slope in a pyrolytic mantle to be $+8 \pm 4$ MPa K^{-1}. Grocholski et al. (2012) estimated $+5.6 \pm 0.8$ MPa K^{-1} based on Tsuchiya's Au scale, which is very similar to the +5 MPa K^{-1} for pure $MgSiO_3$ using the same pressure scale (Hirose et al., 2006a) and therefore likely corresponds to ~+11 MPa K^{-1} with the MgO scale. These results suggest that the Clapeyron slope of post-perovskite phase transition in a natural mantle composition is similar to that in $MgSiO_3$ and may be as high as 11–13 MPa K^{-1}. Given the likelihood of substantial lateral variations in temperature in the D″ thermal boundary layer, there are likely to be substantial depth variations in the phase boundary and any associated seismic velocity changes.

2.05.2.2.5 The stability of $MgSiO_3$ post-perovskite at extreme pressures

The stability of the post-perovskite phase with increasing pressure is important for understanding the internal structure and dynamics of large rocky planets – super-Earth-type exoplanets – which should be relatively abundant and may exist around as many as 23% of stars (Howard et al., 2010). Early studies focused on the internal structure of these planets and on the viability of plate tectonics (Seager et al., 2007; Sotin et al., 2007; Valencia et al., 2006, 2007a,b,c). More recent dynamical modeling studies have included some depth-dependent properties (Tackley et al., 2013), but not the effect of deeper phase transitions, which were considered by van den Berg et al. (2010b). Views on the 'next' phase transition in $MgSiO_3$, the post–post-perovskite transition, are still evolving but the trend toward full dissociation into elementary oxides, MgO and SiO_2 (Umemoto et al., 2006a,b), is unaltered. It just seems that the dissociation process is gradual, not direct. $MgSiO_3$ post-perovskite was first predicted to dissociate into CsCl-type MgO and cotunnite-type SiO_2 at ~11 Mbar (Umemoto et al., 2006b). This prediction was slightly revised after the identification of another polymorph of SiO_2, the Fe_2P-type phase (Tsuchiya and Tsuchiya, 2011; Wu et al., 2011), with the latter being stable at low temperatures but transforming to the cotunnite-type phase at ~6000 K. A more gradual dissociation process was later identified (Umemoto

and Wentzcovitch, 2011). The two-stage dissociation pathway consists in the gradual exsolution of MgO from $MgSiO_3$

$$2MgSiO_3(pPv) \rightarrow MgSi_2O_5(P2_1/c\text{-type}) + MgO(CsCl\text{-type})$$

at ~9 Mbar, followed by full dissociation of $MgSi_2O_5$

$$MgSi_2O_5(P2_1/c\text{-type}) + MgO(CsCl\text{-type}) \rightarrow 2MgO(CsCl\text{-type}) + 2SiO_2(Fe_2P\text{-type})$$

at ~21 Mbar. The new $P2_1/c$-type $MgSi_2O_5$ phase was identified by following dynamical instabilities in $MgSi_2O_5$ in the structure of $CaGe_2O_5$ with space group *Pbam* (Nemeth et al., 2007), a post-titanate-type phase. This phase has 32 atoms per cell, and it has two types of silicon, one ninefold- and eightfold-coordinated, while magnesium is ninefold-coordinated.

This finding raised even more questions about the dissociation process. Could, alternatively, SiO_2 also exsolve gradually? A possible exsolution mechanism is

$$2MgSiO_3(pPv) \rightarrow Mg_2SiO_4(new) + SiO_2(Fe_2P\text{-type})$$

An adaptive genetic algorithm was developed used to search for stable structures with composition Mg_2SiO_4 and to repeat the search for structures with composition $MgSi_2O_5$ (Wu et al., 2014). This search confirmed the stability of the $P2_1/c$-type $MgSi_2O_5$ phase and identified a new high-pressure form of Mg_2SiO_4. This structure is body-centered tetragonal with space group I-42d. The cation configuration of this phase is identical to that of Zn_2SiO_4-II whose space group is I-42d also (Marumo and Syono, 1971). The difference between I-42d-type Mg_2SiO_4 and Zn_2SiO_4-II is in the oxygen arrangement. Mg_2SiO_4 is much more closely packed than Zn_2SiO_4-II. Both Mg and Si atoms in Mg_2SiO_4 are eightfold-coordinated, while Zn and Si atoms in Zn_2SiO_4-II are fourfold (tetrahedrally)-coordinated. The crystal structures of I-42d-type Mg_2SiO_4 and $P2_1/c$-type $MgSi_2O_5$ together with the corresponding local structures are shown in Figure 6.

This enlarged composition space of possible structures now reveals a more complex three-step dissociation process – $MgSiO_3$ post-perovskite first decomposes into two phases at 7.7 Mbar, one rich (poor) and one poor (rich) in SiO_2 (MgO):

$$3MgSiO_3(pPv) \rightarrow Mg_2SiO_4(I\text{-}42d\text{-type}) + MgSi_2O_5(P2_1/c\text{-type})$$

In the presence of Mg_2SiO_4, $MgSi_2O_5$ breaks down into Mg_2SiO_4 and SiO_2 at 12.5 Mbar:

$$Mg_2SiO_4(I\text{-}42d\text{-type}) + MgSi_2O_5(P2_1/c\text{-type}) \rightarrow {}^3/_2\, Mg_2SiO_4(I\text{-}42d\text{-type}) + {}^3/_2SiO_2(Fe_2P\text{-type})$$

The complete dissociation into oxides then takes place at ~30.9 Mbar:

$${}^3/_2\, Mg_2SiO_4(I\text{-}42d\text{-type}) + {}^3/_2SiO_2(Fe_2P\text{-type}) \rightarrow 3MgO(CsCl\text{-type}) + 3SiO_2(Fe_2P\text{-type})$$

This sequence of transitions is shown in Figure 6. The dissociation starts at 8 Mbar and is completed at ~31 Mbar. This pressure range is expected to change somewhat at high temperatures though. This prediction contrasts with the direct dissociation previously predicted at ~11 Mbar (Umemoto et al., 2006b) and the two-step exsolution of MgO predicted between ~9 and 21 Mbar (Umemoto and Wentzcovitch, 2011). Among this latest sequence of dissociation transitions, only the first two are relevant for understanding the mantle of terrestrial exoplanets with up to 10 Earth masses. Mantle pressures in these planets are expected to reach ~14 Mbar and temperatures ~6,000 K (Sotin et al., 2007). In overall, these results suggest that more complex sequences of phase transitions could be found by considering intermediate phases with different compositions. The large ionic (LDA) gaps of at least 5 eV found in all phases suggest that phases with different molar fractions of MgO and SiO_2 with even more complex structures are the most natural candidates for future investigations.

2.05.3 D″ Region and Evidence for Post-Perovskite

Seismological observations have long indicated a relatively simple structure of the lower mantle with smooth P- and S-wave velocity and density increases with depth from the transition zone down to the much more heterogeneous D″ region (see 'Deep Earth Structure'). In the lowermost 300–500 km of the mantle, seismic wave travel times and waveforms indicate reductions in radial velocity gradients, abrupt increases and decreases in velocity, increases in short-period wave scattering, increase in anisotropic properties, and strong lateral gradients in structure. The D″ region has a preponderance of large-scale (degree-2 and degree-3) variations, with two LLSVPs extending upward several hundred kilometers from the CMB beneath the southern Pacific and Africa and high P- and S-wave velocities below the circum-Pacific subduction zones. Strong S-wave and intermittent P-wave velocity increases 100–300 km above the CMB have

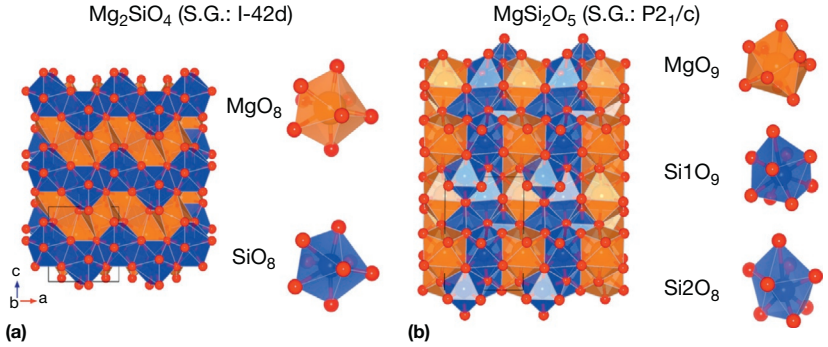

Figure 6 Crystal structures of I-42d Mg_2SiO_4 and $P2_1/c$ $MgSi_2O_5$.

been observed primarily in the high-velocity regions, which are generally thought to have lower than average temperatures due to the downwelling of oceanic lithosphere. A widely observed strong S-wave velocity increase of 2–3% several hundred kilometers above the CMB is often designated the D″ discontinuity. It was more than 20 years after its initial observation by Lay and Helmberger (1983) that the post-perovskite phase transition first provided a possible explanation for this structure. The expectation that perovskite-to-post-perovskite transition will occur at lower pressure for lower temperatures suggests that any associated seismological signature should be found at shallower depth in higher-velocity regions. The seismological structures detected in the lowermost mantle require both thermal and chemical heterogeneities and dynamical processes that sustain the complexity. The consideration of possible manifestations of deep mantle post-perovskite must allow for significant variations in temperature and composition (Lay and Garnero, 2007).

2.05.3.1 Elasticity

The post-perovskite transition in $MgSiO_3$ at conditions similar to those expected at the D″ discontinuity offers a candidate framework for interpreting the properties of this region. However, the complexity of the D″ region and the uncertain local mineral composition raise questions about its geophysical significance. The contrast between the elastic properties of perovskite and post-perovskite is critical to establishing the presence of post-perovskite in this region. In particular, one would like to verify whether (i) shear and longitudinal velocity changes across the D″ discontinuity and (ii) the anticorrelation between shear and bulk velocity heterogeneities in this region can be better understood by invoking the post-perovskite transition.

The elasticity of perovskite and post-perovskite phases has been calculated by first principles using two complementary techniques: MD (Oganov et al., 2001; Stackhouse and Brodholt, 2007) and QHA in conjunction with phonon frequencies (Wentzcovitch et al., 2004, 2009). The QHA method offers detailed information in a continuum in pressure and temperature parameter space and is very useful to compute pressure and temperature gradients and lateral heterogeneities in great detail.

The elastic coefficients of $MgSiO_3$ post-perovskite are remarkably different from those of perovskite (see **Figure 7**). Post-perovskite is a layered structure, expands more anisotropically, and has more complex pressure- and temperature-dependent elastic behavior than perovskite (Tsuchiya et al., 2004b). However, its aggregate moduli do not differ dramatically from those of perovskite. The adiabatic bulk moduli of both phases, K (**Figure 8**), are similar at $P > 80$ GPa. This is also true for other thermodynamic properties (Tsuchiya et al., 2005a). The shear modulus, G, of post-perovskite is larger and has larger pressure and temperature gradients at deep lower mantle conditions. Considering that post-perovskite is ~1.5% denser than perovskite at D″ conditions, the resulting effect on velocities are easy to rationalize (see **Figure 9**). Because of G, post-perovskite's V_S is larger and has larger pressure and temperature gradients. The longitudinal velocity, V_P, is a little larger and has slightly larger gradients because of G as well (see **Figure 9**). In contrast, the bulk velocity, V_Φ, is a smaller than that of perovskite because of their similar K and the larger density (ρ) of post-perovskite. Although minor differences remain, these results are in general agreement with those based on first-principles MD (Oganov et al., 2001; Stackhouse and Brodholt, 2007).

2.05.3.2 Velocity Jumps and Lateral Heterogeneity

These predicted contrasts between perovskite and post-perovskite velocities manifest across the phase transitions as a positive jump in V_S, negative jump in V_Φ, and small positive jump in V_P (see **Figure 10**) (Wentzcovitch et al., 2006; Wookey et al., 2005). These results are consistent with seismic velocity jumps observed 200–300 km above the core–mantle boundary in certain places but most easily detected beneath regions of past subduction, presumably cold places, such as beneath Central America (e.g., Hutko et al., 2008, 2009; Lay and Helmberger, 1983). There, $\Delta V_S > \Delta V_P$ and $\Delta V_S \sim 2$–3% are observed, but this observation is clearly a regional property of a notably heterogeneous layer (Garnero, 2004; Lay and Garnero, 2004; Lay et al., 1998b, 2004; Wysession et al., 1998).

A well-known property of D″ revealed by early global tomography models (e.g., Masters et al., 2000) is anticorrelation between large-scale lateral V_Φ and V_S heterogeneities. The likely cause(s) of heterogeneities is best addressed by comparing simultaneously the magnitude of average heterogeneity ratios such as $R_{S/P} = (\partial \ln V_S / \partial \ln V_P)_P$ and $R_{\Phi/S} = (\partial \ln V_\Phi / \partial \ln V_S)_P$, to computational predictions or experimental measurements at relevant conditions (Karato and Karki, 2001). It is known that in the shallow lower mantle, $R_{S/P} \sim 2.3$ and $R_{\Phi/S} \sim 0.0$, whereas in D″, $R_{S/P} \sim 3.4$ and $R_{\Phi/S} \sim -0.2$ (Masters et al., 2000). Heterogeneity ratios produced by isobaric temperature changes in pure post-perovskite and perovskite aggregates are displayed in **Figure 11(a)** and **11(b)** along with the seismic parameters extracted from Masters et al. (2000) and reported by Karato and Karki (2001). In pure perovskite aggregates, $R_{S/P}$ increases with pressure and temperature but reaches at most 2.3 at 135 GPa and 4000 K (**Figure 11(b)**), whereas $R_{\Phi/S}$ is approximately pressure-independent and slightly decreases with temperature to reach 0.16 at the same conditions (see **Figure 12(b)**). In post-perovskite, $R_{S/P}$ decreases with pressure, but because of its larger $(\partial G/\partial T)_P$, it increases more rapidly with temperature to reach ~2.5 at the same conditions (**Figure 11(a)**). $R_{\Phi/S}$ is smaller for post-perovskite, 0.1, at these conditions (see **Figure 12(a)**). It has been argued that anelasticity, anisotropy, and lateral variations in calcium content in the deepest mantle might be necessary to produce large values for $R_{S/P}$ and negative values for $R_{\Phi/S}$, unless there is a phase transformation (Karato and Karki, 2001).

Figures 11(c) and **12(c)** compare these heterogeneity ratios caused by the post-perovskite transition along the calculated phase boundary (**Figure 5**). $R_{S/P} > 6$ and $R_{\Phi/S} < -0.5$ results from this phase change. This indicates that lateral variation in post-perovskite abundance can enhance these seismic parameters as observed. This effect was estimated by Oganov and Ono (2004) assuming the temperature dependences of perovskite and post-perovskite velocities were the same. Coexisting secondary phases such as ferropericlase and $CaSiO_3$ perovskite will decrease these anomaly ratios. Besides, the post-perovskite

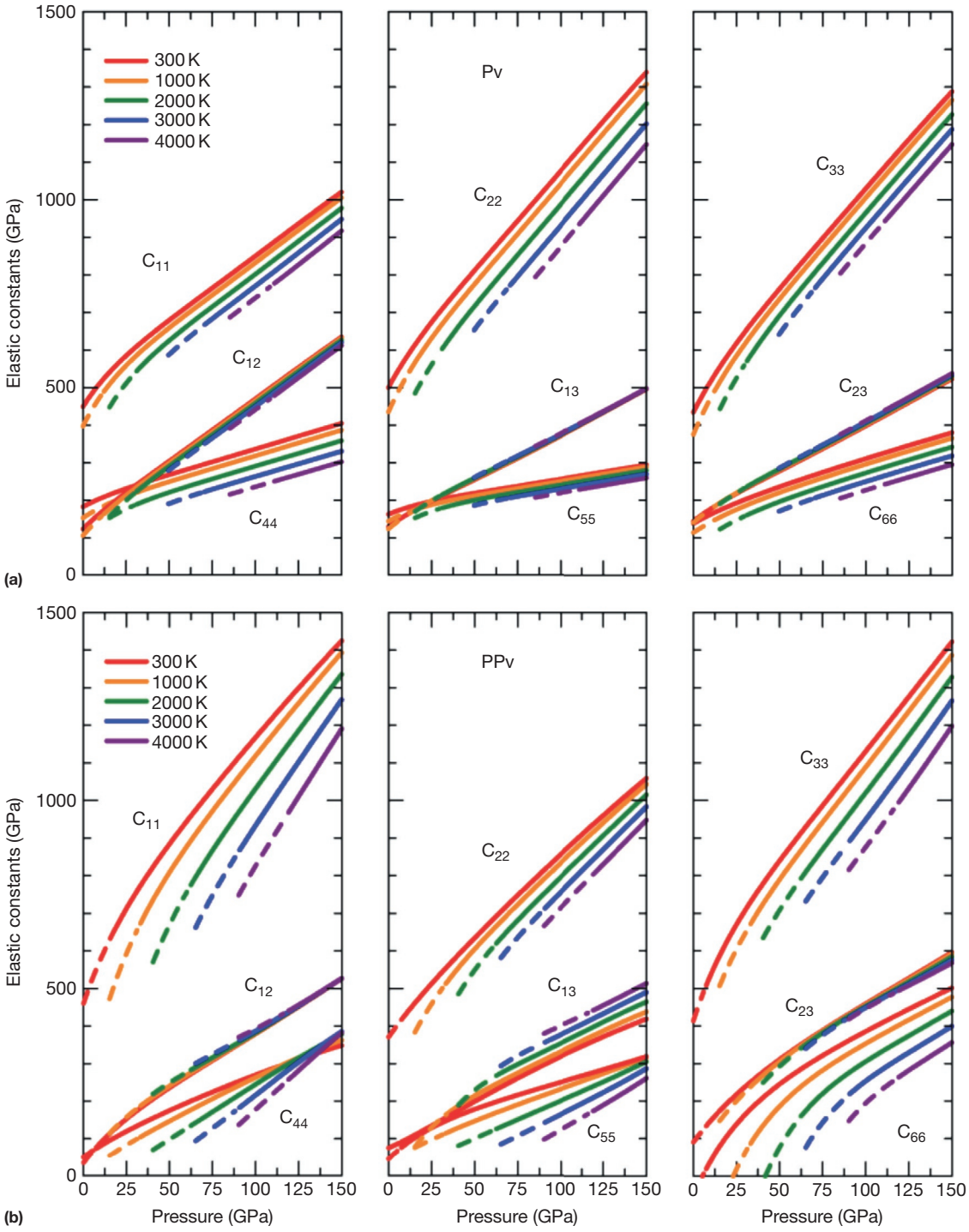

Figure 7 Elastic coefficients of (a) perovskite and (b) post-perovskite obtained using LDA. Reproduced from Wentzcovitch RM, Justo JF, Wu Z, da Silva CRS, Yuen D, and Kohlstedt D (2009) Anomalous compressibility of ferropericlase throughout the iron spin crossover. *Proceedings of the National Academy of Sciences of the United States of America* 106: 8447–8452.

phase transition on solid solutions should open a binary loop that will smooth these velocity contrasts (Grocholski et al., 2012). Nevertheless, the effect of lateral variations in post-perovskite abundance on these seismic parameters seems very robust and indicative of the presence of post-perovskite in the D″ region, as later supported by the statistical analysis of Trampert et al. (2004).

As pointed out earlier, the topography of D″ is consistent with a solid–solid phase transition with positive Clapeyron slope (~4–10 MP K^{-1}) induced by lateral temperature

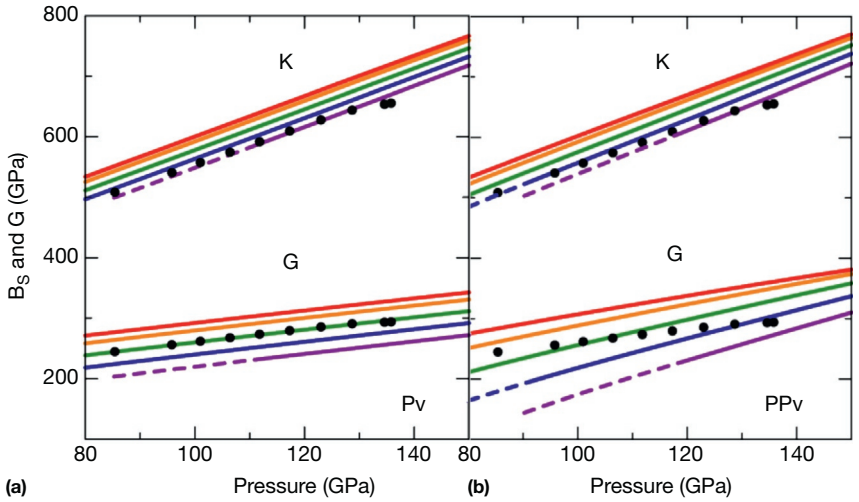

Figure 8 Adiabatic bulk modulus (K) and shear modulus (G) of (a) perovskite and (b) post-perovskite. Same color code as **Figure 7** applies.

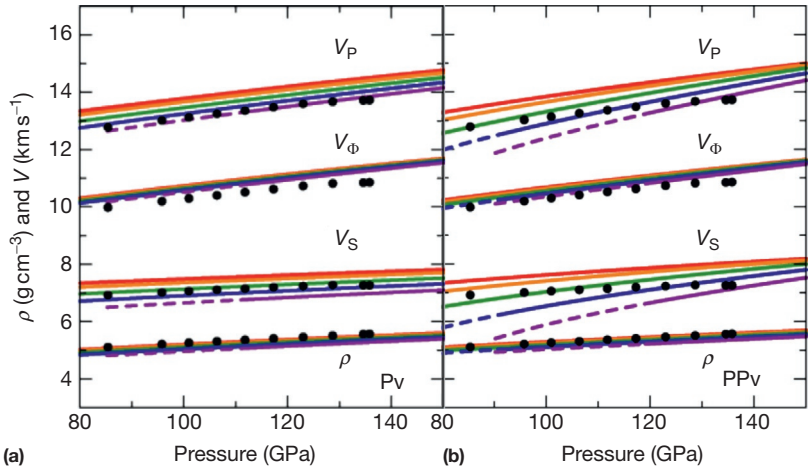

Figure 9 Isotropic longitudinal (V_P), bulk (V_φ), and shear (V_S)-wave velocities and density (ρ) of (a) perovskite and (b) post-perovskite. Filled circles in (a) and (b) are PREM values (Dziewonski and Anderson, 1981) for comparison. Same color code as **Figure 7** applies.

variations (Sidorin et al., 1999). The anticorrelation between V_Φ and V_S heterogeneities and their geographic locations are also consistent with this assumption if the post-perovskite phase is abundant in the D″ region. Beneath the central Pacific, V_Φ is faster and V_S is slower than their spherical averages, whereas beneath the circum-Pacific, the opposite is observed. These regions are generally considered to be hotter and colder than average, respectively. The positive Clapeyron slope suggests that hotter regions should contain less post-perovskite and therefore have faster V_Φ and slower V_S, whereas colder regions should contain more post-perovskite and have slower V_Φ and faster V_S, as observed. Lateral variations in phase abundances alone do not account for the complex nature and properties of D″. Nevertheless, this perspective is helpful as a reference starting model to attempt understanding the D″ region. Secondary phases and minor element partitioning on the post-perovskite phase boundary and on aggregate elasticity, particularly the important effect of iron (Mao et al., 2005), must be addressed first before a more quantitative reference mineralogical model for D″ is developed. The origin of the negative $R_{\Phi/S}$ above D″ indicated in Figure 12 is also unclear.

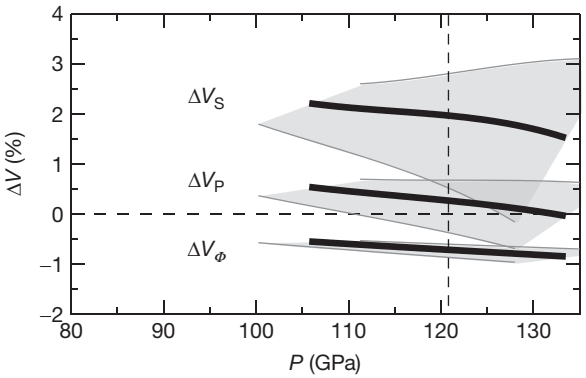

Figure 10 Velocity jumps across the phase boundary shown in **Figure 5**. Thick black lines represent the jumps at the center of the phase boundary with a density functional theory-related uncertainty of ~10 GPa. Shaded areas are possible values throughout the boundary uncertainty domain. Open triangles and squares, respectively, are results from molecular dynamics simulations at 135 GPa and 4000 K and 136 GPa and 3000 K. The vertical dashed line indicates the pressure at approximately the top of the D″ discontinuity.

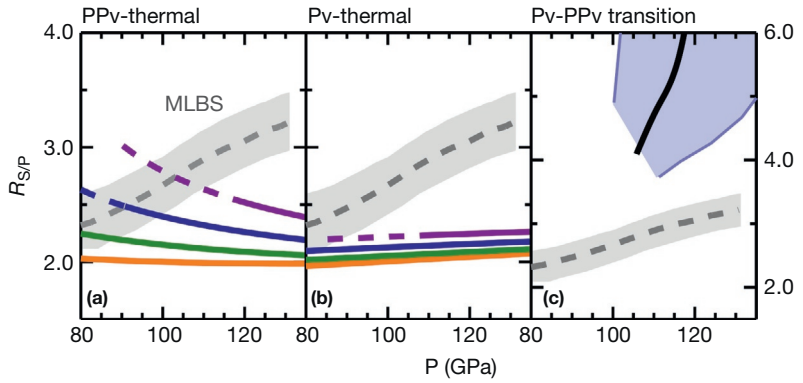

Figure 11 Heterogeneity ratio $R_{S/P} = (\partial \ln V_S / \partial \ln V_P)_P$ caused by lateral temperature variations (a) in perovskite, (b) in post-perovskite, and (c) across the phase boundary. Blue-shaded area in (c) is related with the uncertainty in the post-perovskite phase boundary shown in **Figure 5**. Seismic values are extracted from Masters et al. (2000).

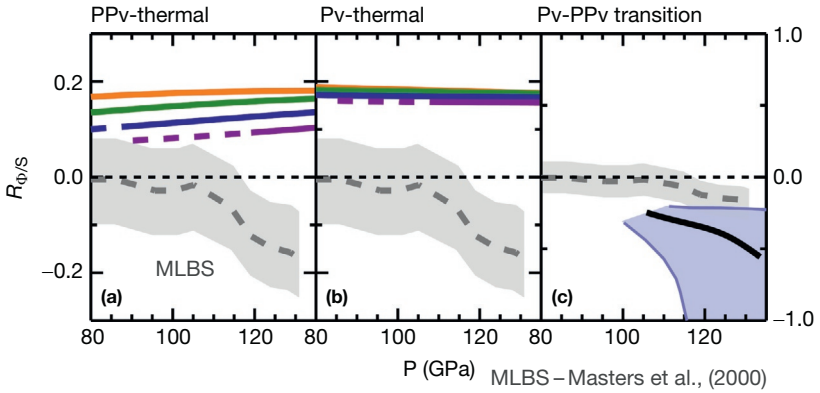

Figure 12 Heterogeneity ratio $R_{\Phi/S} = (\partial \ln V_\Phi / \partial \ln V_S)_P$ caused by lateral temperature variations (a) in perovskite, (b) in post-perovskite, and (c) across the phase boundary. Shaded areas have the same meaning as in **Figure 11**.

There is indication that this effect could, for instance, originate in lateral temperature variations in the spin crossover in ferropericlase (Wu and Wentzcovitch, 2013; Wu et al., 2013), but the extent to which this can be explained is still not clear.

These results suggest that a third heterogeneity ratio, $R_{\rho/S} = (\partial \ln \rho / \partial \ln V_S)_P$, should be positive for the phase transition and perhaps increase with depth in the lowermost mantle (see lowest portion of **Figure 13**), unless other effects or chemical heterogeneities (Humayun et al., 2004; Karato and Karki, 2001; Lay et al., 2004) occur simultaneously. Some 3D density models do not support this prediction (Ishii and Tromp, 1999), whereas others do (Romanowicz, 2001). Estimates of this parameter obtained by joint inversions of seismic and geodynamic data also tend to offer a positive ratio (Forte et al., 1994). It appears that until a clear consensus on the 3D structure of the density in the mantle is reached, this issue will remain open. Recently, it has been pointed out that an average excess density of 0.4% in the lowermost mantle is admissible within normal mode constraints (Garnero et al., 2004), in agreement with our expectations.

2.05.3.3 Anisotropy

Significant shear-wave polarization anisotropy has been detected in the lowermost mantle, in particular under the circum-Pacific regions, where the horizontally polarized S-wave velocity (V_{SH}) is faster by 1–3% than the vertically polarized S-wave velocity (V_{SV}) (e.g., Section 1.19; Lay et al., 1998a; Panning and Romanowicz, 2004). The overlaying lower mantle appears to have less anisotropic effects on seismic waves, indicating that D″ structure has distinct anisotropic properties. Since single-crystal elastic anisotropy of post-perovskite is strong, such seismic anisotropy is plausibly attributed to the lattice-preferred orientation (LPO) of post-perovskite, although the anisotropy of ferropericlase has been also stressed (Wentzcovitch et al., 2006; Yamazaki and Karato, 2002; Yamazaki et al., 2009).

The LPO of a mineral depends on its deformation mechanisms, particularly the activated slip systems. For post-perovskite, the layering plane (0 1 0) was originally suggested to be a dominant slip plane from crystallographic considerations (Iitaka et al., 2004; Murakami et al., 2004; Oganov and Ono, 2004). Indeed, the (0 1 0) slip plane is supported by the deformation experiments on $CaIrO_3$ analog (Miyajima et al., 2006; Niwa et al., 2007). Other slip systems such as (1 0 0) or (1 1 0) have been also suggested by both theory and experiments on $MgSiO_3$ and $MgGeO_3$ (Merkel et al., 2006, 2007; Oganov et al., 2005). Walte et al. (2009) pointed out that the earlier deformation experiments in a DAC by Merkel et al. (2006, 2007) observed 'phase transformation texture,' which is different from 'deformation texture.'

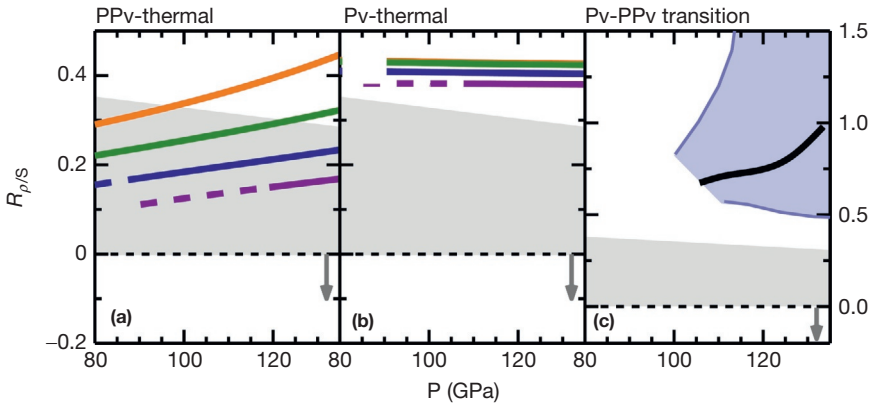

Figure 13 Heterogeneity ratio $R_{\rho/S} = (\partial \ln \rho / \partial \ln V_S)_P$ caused by lateral temperature variations (a) in perovskite, (b) in post-perovskite, and (c) across the phase boundary. Shaded areas have the same meaning as in **Figure 11**.

More recent experiments by Okada et al. (2010) first demonstrated that (0 0 1) is a dominant slip plane of post-perovskite using $MgGeO_3$ analog. Miyagi et al. (2010) argued that the deformation texture of $MgSiO_3$ post-perovskite is the same as the transformation texture and concluded that (0 0 1) is the slip plane. This is consistent with first-principles results (Wentzcovitch et al., 2006) (see **Figure 14**). Hirose et al. (2010) performed high-temperature deformation experiments on $MnGeO_3$ post-perovskite and confirmed the (0 0 1) slip plane is dominant at lower mantle *P*–*T* conditions.

For the (0 0 1) slip plane, observed seismic anisotropy can be reconciled with the LPO of post-perovskite, because the perfect alignment of post-perovskite with (0 0 1) parallel to the horizontal plane produces 8–15% shear splitting, larger than for any other slip system. The maximum 3% polarization anisotropy observed in the D″ layer can be accounted for by LPO of post-perovskite with less than 25% alignment on the basis of the elastic constants predicted by Stackhouse and Brodholt (2007).

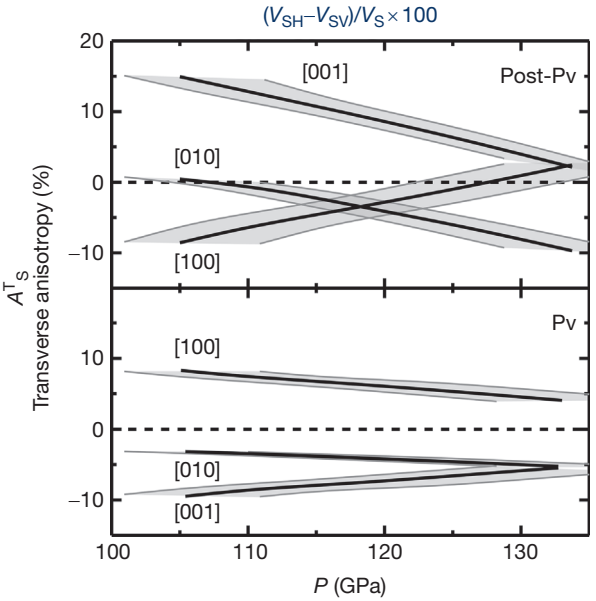

Figure 14 Shear-wave splittings, $(V_{SH} - V_{SV})/V_S$, in $MgSiO_3$ post-perovskite and perovskite, along the thermodynamic phase boundary shown in **Figure 5** with respective uncertainties. These results correspond to horizontally (V_{SH}) and vertically (V_{SV}) polarized shear waves propagating in transversely isotropic aggregates with three possible alignments of the major crystalline axes along the vertical direction.

2.05.4 Transport Properties

2.05.4.1 Viscosity

The rheological properties of $MgSiO_3$-rich post-perovskite are of importance to the dynamics in the D″ layer. Relevant experiments on the deformation of post-perovskite and on its grain growth rate are difficult to perform at the lowermost mantle high *P*–*T* conditions. Thus, extensive experiments using the $CaIrO_3$ analog have been made at low pressures (<3 GPa).

Yoshino and Yamazaki (2007) examined grain growth kinetics of $CaIrO_3$ perovskite and post-perovskite aggregates and found that the grain growth of post-perovskite is distinctly slower than that of perovskite. Such sluggish grain growth may be caused by the strongly anisotropic shape of post-perovskite. Grain-size-sensitive diffusion creep is the dominant deformation mechanism of post-perovskite, at least right after the phase transformation in descending slabs, and the initially small grain size may induce significant softening of the D″ layer. The slow growth rate of post-perovskite maintains its small grain size and resulting weakness.

Hunt et al. (2009) carried out deformation experiments on both perovskite and post-perovskite in the $CaIrO_3$ system below 3 GPa. Their results demonstrated that post-perovskite is at least five times weaker, and possibly significantly more so, than perovskite. They performed experiments with a grain size sufficiently large to be outside the field of grain-size-sensitive plasticity. This confirms that weakening is not an effect of grain-size reduction.

Theoretical calculations by Ammann et al. (2010) demonstrated that diffusion of Mg^{2+} and Si^{4+} in post-perovskite is extremely anisotropic. Assuming diffusion creep is a dominant deformation mechanism of post-perovskite in the D″ layer, the

fast diffusion direction will render post-perovskite up to four orders of magnitude weaker than perovskite.

These studies suggest strong viscosity contrast between perovskite and post-perovskite. However, the inference of very weak post-perovskite remains debated, with other investigations arguing for a neutrally viscous or even a stronger post-perovskite (Karato, 2011). The rheology of post-perovskite has a first-order influence on mantle dynamics and thermal evolution (Cizkova et al., 2010; Nakagawa and Tackley, 2006; Tosi et al., 2010). If post-perovskite in the mantle is actually very weak, it significantly amplifies the influence relative to that calculated for post-perovskite with neutral viscosity.

2.05.4.2 Thermal Conductivity

The thermal boundary layer at the bottom of the mantle is a region where heat is transported predominantly by conduction from the core into the mantle. Conductive heat is given by the product of temperature gradient and thermal conductivity of the lowermost mantle materials. With known thermal conductivity values, one can estimate heat flow from thermal gradient (see a review by Lay et al., 2008), or vice versa.

Researchers often assume a thermal conductivity, k, of $10\,\mathrm{W\,m^{-1}\,K^{-1}}$ for the lowermost mantle, based on Stacey (1992). The thermal conductivity is the sum of lattice component and radiative component. The radiative part of the thermal conductivity of perovskite has been measured at high pressure by Goncharov et al. (2008) and Keppler et al. (2008). The former study reported only $\sim 0.5\,\mathrm{W\,m^{-1}\,K^{-1}}$ at the top of D″ layer and possibly $\sim 1\,\mathrm{W\,m^{-1}\,K^{-1}}$ at the CMB (radiative thermal conductivity increases with increasing temperature), which is relatively small compared to lattice contribution. On the other hand, the latter experiments demonstrated that the radiative component contributes greater than $5\,\mathrm{W\,K^{-1}\,m^{-1}}$ at the CMB, suggesting that the conventional value of $10\,\mathrm{W\,m^{-1}\,K^{-1}}$ underestimates the actual thermal conductivity. The source of inconsistency between these two studies is not clear, and thus, the radiative part of the thermal conductivity for perovskite (and post-perovskite) remains an open question.

For the lattice component of thermal conductivity, Osako and Ito (1991) obtained the conductivity of $MgSiO_3$ perovskite from the measurements of thermal diffusivity at ambient condition (conductivity is calculated from diffusivity, density, and heat capacity). Both high-pressure measurements and calculations have commenced recently. Manthilake et al. (2011) measured lattice thermal diffusivity of $MgSiO_3$-rich perovskite and (Mg,Fe)O ferropericlase up to 26 GPa and 1073 K in a multi-anvil apparatus, the pressure corresponding to the uppermost lower mantle. They also examined the effect of chemical impurity, demonstrating that only 3 mol% Fe and 2 mol% Al in perovskite significantly diminish the diffusivity at 300 K although less at higher temperatures of the lower mantle. Relatively large extrapolation of their measurements provides $k - 8.4 \pm 1.2\,\mathrm{W\,m^{-1}\,K^{-1}}$ at the CMB, comparable to the conventional value, assuming radiative contribution is small. More recently, Ohta et al. (2012b) measured thermal diffusivity of $MgSiO_3$ perovskite and post-perovskite up to 144 GPa at room temperature, by applying thermoreflectance method in a DAC (Yagi et al., 2011). Considering the value for ferropericlase and the temperature effect of reducing the conductivity of perovskite from Manthilake et al. (2011), Ohta et al. estimated a lattice conductivity of $11\,\mathrm{W\,m^{-1}\,K^{-1}}$ at the CMB if perovskite is present there. On the other hand, Ohta et al. (2012b) also found that $MgSiO_3$ post-perovskite exhibits 60% higher thermal diffusivity than perovskite at equivalent condition, approximately consistent with the measurements of the $CaIrO_3$ analog that indicate that the thermal conductivity of post-perovskite phase is nearly twice as high as that of perovskite phase (Hunt et al., 2012; Keawprak et al., 2009).

The thermal conductivity of MgO has been calculated at lower mantle P–T conditions in recent studies (de Koker et al., 2012; Haigis et al., 2012; Stackhouse et al., 2010; Tang and Dong, 2010). All such calculations show very high conductivity of MgO, far exceeding the values of perovskite, although the results vary from ~ 80 to $150\,\mathrm{W\,m^{-1}\,K^{-1}}$ at the CMB. The conductivity of $MgSiO_3$ perovskite was also calculated by Haigis et al. (2012), predicting $10.8\,\mathrm{W\,m^{-1}\,K^{-1}}$ for a mixture of $MgSiO_3$ perovskite + MgO, again consistent with the traditional value. More recent calculations by Dekura et al. (2013) showed somewhat lower value of about $5\,\mathrm{W\,m^{-1}\,K^{-1}}$ for peridotitic material at the CMB. The calculations by Haigis et al. (2012) also demonstrated that the thermal conductivity $MgSiO_3$ post-perovskite is $167 \pm 25\,\mathrm{W\,m^{-1}\,K^{-1}}$ at 135 GPa and 300 K, which is much higher than $65 \pm 14\,\mathrm{W\,m^{-1}\,K^{-1}}$ measured by Ohta et al. (2012b). Ohta et al. assumed a temperature effect the same as that for perovskite, while Haigis et al. predicted a much larger temperature effect. As a result, the former concluded 60% higher conductivity than perovskite, but the latter suggested very similar conductivity.

These results are summarized in **Table 1**. If $MgSiO_3$-rich perovskite is present right above the CMB, the thermal conductivity of the thermal boundary layer may be $8–11\,\mathrm{W\,m^{-1}\,K^{-1}}$ or higher if radiative conductivity is $\sim 5\,\mathrm{W\,m^{-1}\,K^{-1}}$. On the other hand, if post-perovskite is the principal mineral in the thermal boundary layer, the conductivity can be much larger, depending on the temperature effect on the conductivity of post-perovskite.

2.05.4.3 Electric Conductivity

Relatively high electric conductivity of the lowermost mantle can cause strong electromagnetic coupling between the solid mantle and liquid core, which may play an important role in modulating the length of a day (rotational speed of the Earth's crust and mantle) (Holme, 1998) and precession of the Earth's rotation axis (Buffett et al., 2000). Enhanced electric conductivity of post-perovskite relative to perovskite was originally suggested by measurements for the $CaIrO_3$ analog (Ohgushi et al., 2006). This is because electrons are expected to be more conducting within the a–c planes owing to the layered structure of post-perovskite. Ono et al. (2006) considered high electric conductivity of $MgSiO_3$-rich post-perovskite in the Earth's lowermost mantle, based on earlier shock-wave measurements of Al_2O_3 with post-perovskite structure. They also discussed the idea that a highly conductive lowermost mantle could be the cause of changes in the length of day.

The electric conductivity of the lower mantle has been unknown until recently. Xu et al. (2000) measured the conductivity of perovskite under the topmost lower mantle

conditions and modeled the lower mantle conductivity profile by extrapolating the experimental data to much higher P and T. However, subsequently discovered high-spin to low-spin crossovers for iron (Badro et al., 2003) in (Mg,Fe)O ferropericlase, perovskite, and post-perovskite (Murakami et al., 2004) are now known to affect the electric conductivity to a great extent. Iron spin crossover occurs in ferropericlase in the middle to deep lower mantle (Lin et al., 2007a,b; Tsuchiya et al., 2006). While the spin state of ferrous iron in perovskite has been controversial (Badro et al., 2004; McCammon et al., 2008; Umemoto et al., 2010), it is generally accepted that ferric iron undergoes spin crossover in the mid-lower mantle (Stackhouse et al., 2007; Zhang and Oganov, 2006).

Lin et al. (2007b) and Ohta et al. (2007) first demonstrated the effect of iron spin crossover on the electric conductivity of (Mg,Fe)O ferropericlase experimentally; the conductivity increased with increasing pressure but suddenly diminished above ~70 GPa at room temperature, similar to the pressure range of spin crossover in ferropericlase. The electric conduction in high-spin ferropericlase is dominated by a small-polaron process of electron hopping between ferrous and ferric iron sites (Dobson and Brodholt, 2000). The unpaired electrons in the 3d orbital play important roles in this process, but the number of unpaired electrons of ferric iron decreases from four to zero at the spin crossover, thus resulting in a marked reduction in the conductivity. Similar reduction in the electric conductivity of Fe-bearing $MgSiO_3$ perovskite has been also demonstrated at both 300 K (Ohta et al., 2010a,b) and high temperatures (Ohta et al., 2008b). These are likely caused by the spin crossover in ferric iron.

The electric conductivity of $(Mg_{0.9}Fe_{0.1})SiO_3$ post-perovskite has been measured to be on the order of $10^2\,S\,m^{-1}$, higher by three orders of magnitude than that of perovskite with iron in the low-spin state (Ohta et al., 2008b). This is attributed to the shorter Fe–Fe distance in post-perovskite structure, in which Mg and Fe form sheets interlayering with SiO_6 (Figure 2). The conductivity of a peridotitic mantle material was also measured in a wide P–T range that covers almost all lower mantle conditions (Ohta et al., 2010a). The results showed $10^{1.5}\,S\,m^{-1}$ at the base of the mantle. This is somewhat lower than that of single-phase $(Mg_{0.9}Fe_{0.1})SiO_3$ post-perovskite, because iron content in post-perovskite coexisting with ferropericlase in a pyrolytic bulk composition is less than 5 mol% (Murakami et al., 2005; Sinmyo et al., 2011). Alternatively, subducted MORB crust (Ohta et al., 2010a) or metallic FeO possibly exsolved from liquid outer core with cooling (Frost et al., 2010; Ohta et al., 2012a,b) will have enhanced electric conductivity near the base of the mantle and may be responsible for strong electromagnetic coupling between the solid mantle and liquid core.

2.05.5 Geodynamic Consequences of Post-Perovskite

The role of phase transitions in mantle dynamics has historically been thought to be limited to the upper mantle, because until 10 years ago, only the olivine to spinel and the spinel to perovskite transitions were viewed as important. Before the discovery of post-perovskite, researchers focused on the issue of layered versus whole-mantle convection in the presence of phase transitions (Christensen and Yuen, 1984, 1985; Honda et al., 1993; Schubert et al., 1975; Tackley et al., 1993) and the so-called avalanche events associated with the phase transition at 660 km depth. This phenomenon, first found by Christensen and Yuen (1985), in 2D models generated much greater attention in 3D (Honda et al., 1993; Tackley et al., 1993) and has attracted the attention of many geochemists (Allegre, 1997).

When the discovery of post-perovskite transition came along, it was recognized that this phase transition is fundamentally different from other mantle phase transitions because of its proximity to the CMB. The dynamical situation resembles the situation of the spinel to perovskite transition in the Martian mantle in which that phase transition may lie very close to the Martian CMB (Breuer et al., 1997; Harder and Christensen, 1996; Weinstein, 1995). Indeed, in the Earth's mantle, post-perovskite may act as a gatekeeper for mantle circulation descending to the CMB.

The D″ region has long been recognized as prone to dynamical instabilities because of the thermal boundary layer above the CMB (Jones, 1977; Stacey and Loper, 2007; Yuen and Peltier, 1980). The implications of the post-perovskite interpretation of the D″ layer, with the transition having a steep positive Clapeyron slope, are quite profound for the dynamics of the deep mantle. The rheology of post-perovskite may also be non-Newtonian and viscosity may be lower than that of perovskite because of the large stresses present at the boundary layer of mantle convection.

2.05.5.1 Dynamical Effects of Post-Perovskite in Earth

Geophysicists have examined the influence of post-perovskite on both thermal and thermochemical convection (Tackley et al., 2007; Yuen et al., 2007). **Figure 15** shows the situation that arises for two Clapeyron slopes that depend on

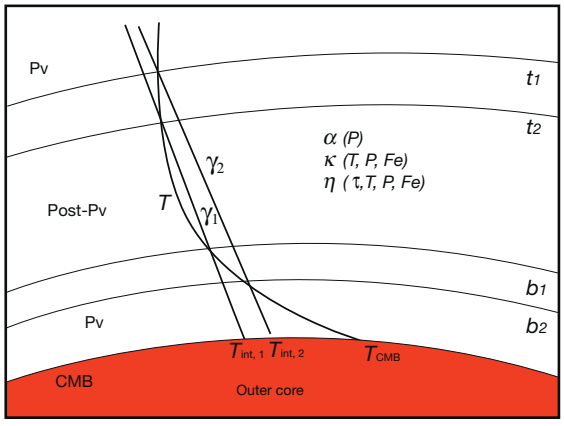

Figure 15 The intersections of the local one-dimensional geothermal with the Clapeyron slopes. T-int marks the temperature of the post-perovskite transition at the core–mantle boundary. The relative positioning between T-int and T-cmb determines whether double-crossing of the geotherm with the phase boundary occurs. Symbols t1, t2, b1, and b2 indicate the top and bottom crossings. α, κ, and η represent, respectively, the thermal expansivity, thermal diffusivity, and viscosity of the lower mantle, and they depend on thermodynamic and chemical variables.

composition or how they would be crossed by a temperature curve associated with a thermal boundary layer above the CMB. We note that because of the uncertainties of the physical parameters, such as the depth variations of thermal expansivity and bulk moduli with depth, it is very difficult to ascertain the relative dynamical importance of each of these factors. With the post-perovskite transition dependent on composition, a great variety of complex behavior may arise, producing structures, such as the multiple crossings of the temperature curve by the two different types of post-pervoskite transition (see **Figure 15**, where t1, t2, b1, and b2 are the four intersections due to compositionally dependent phase boundaries).

The nature of double-crossing of the Clapeyron slope by the local geotherm was recognized early on by Hernlund et al. (2005) who emphasized at that time that the post-perovskite phase boundary can be employed to constrain many important thermal parameters in solid-earth geophysics, such as its phase change location relative to the melting curve of candidate mantle materials. This hypothesis has prompted seismological ventures into relating imaged structures in the D″ layer as thermal and compositionally influenced post-perovskite phase transitions, with attendant absolute temperatures and heat flow estimates (Hutko et al., 2006; Lay et al., 2006; van der Hilst et al., 2007).

From a dynamical standpoint, the 1.5% density change of the post-perovskite transition being may have impact on the local dynamics. This density change is equivalent to more than a thousand degree change in thermal buoyancy, because of the relatively low thermal expansion coefficient of around 10^{-6} in the deep lower mantle. Up to now, this dynamical effect has not been explored for post-perovskite transition at all and requires further examination. Latent heat effects can potentially be important as a feedback mechanism for exothermic phase transitions when coupled with variable viscosity and viscous heating (Steinbach and Yuen, 1994) and would require more investigation especially for the possibly low-viscosity post-perovskite regions in the deep mantle (Ammann et al., 2010; Cizkova et al., 2010).

The dynamical influences of the phase boundary distortions are illustrated schematically in **Figure 16** by a sketch of the phase boundary of post-perovskite (dashed curve) in the cold downwellings and hot upwellings. For temperature at the CMB greater than the temperature of the intercept in the post-perovskite transition, we note that beneath hot plumes, there can exist a patch of hot perovskite. Only as the Earth cools off does the perovskite hole disappear and become filled with post-perovskite. The buoyancy of the hot plumes is increased by the deflection of the lighter perovskite phase downward. In the downwelling, we see also the greater negative buoyancy provided by the phase boundary being pushed upward by the negative thermal contrast. For isotherm T3, there may be another zone of perovskite right above the CMB, delineating what is now called as the 'double-crossing' phenomenon (Hernlund et al., 2005). A Clapeyron slope dP/dT of $\sim$10 MPa K^{-1} can cause undulations of $\sim$100 km in the depth of the phase boundary for thermal perturbations of several hundred degrees.

Electric conductivity increases dramatically across the post-perovskite phase boundary (Ohta et al., 2010b) and aids the leakage of core electric currents to the mantle that can promote enhanced Joule heating at different sites over the CMB, following magnetic jerk events. But of greater dynamical interests are the thermal conductivity and viscosity of post-perovskite, which may, respectively, increase by around 50% and decrease by a factor of 50–100, as discussed in the preceding text. These properties would be conducive to the development of small-scale convection within the D″ layer (Cizkova et al., 2010; Samuel and Tosi, 2012; Schott et al., 2002).

From a dynamical standpoint, what new issues has the post-perovskite transition raised? First of all, we expect that the exothermic character of the post-perovskite transition should tend to promote instability in the D″ layer, increasing the heat flow and interior mantle temperature and increasing the number and time dependence of mantle plumes. Some of these predictions were confirmed by Nakagawa and Tackley (2004) for constant physical properties. **Figure 17** shows a

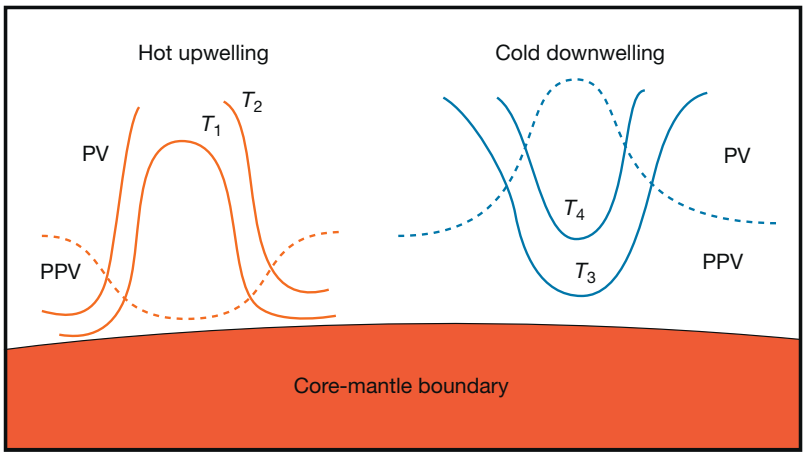

Figure 16 Schematic diagram showing the undulations of the phase boundary of the perovskite-to-post-perovskite transition due to hot upwellings and cold downwellings. T1, T2, T3, and T4 are the isotherms associated with the two types of flow. Dashed curves show the undulations of the phase boundaries. There are an additional positive buoyancy for the upwelling and an additional negative buoyancy associated with the downwelling because of the positive Clapeyron slope of the post-perovskite transition (Schubert et al., 1975).

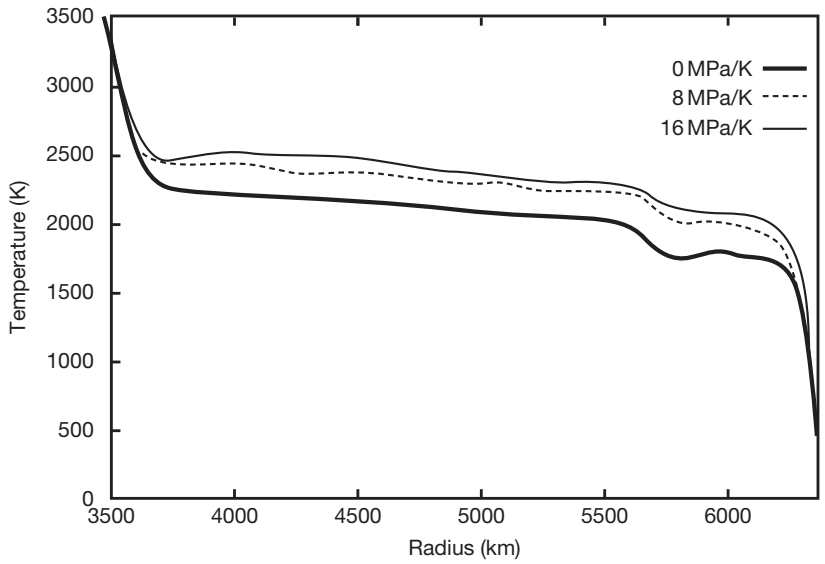

Figure 17 Time and horizontally averaged one-dimensional temperature profiles taken from two-dimensional Cartesian simulations of Nakagawa and Tackley (2004). A comparison is made for no post-perovskite transition to two different values of the Clapeyron slope from 8 to 16 MPa K^{-1}. The temperature increases in the interior from the presence of the post-perovskite transition.

comparison of the time-averaged vertical temperature profiles for three different cases: one without the post-perovskite transition, the second with a Clapeyron slope of 8 MPa K^{-1}, and the third with a slope of 16 MPa K^{-1}. There is an increase in the interior temperature with increasing Clapeyron slope, with a difference of 400 K between the reference case (no post-perovskite) and the case with the steepest Clapeyron slope. A more realistic model with variable viscosity would act to decrease the temperature difference because of negative buffering feedback from temperature-dependent viscosity (Tozer, 1972). The enhanced time dependence of boundary layer instabilities induced by the presence of the post-perovskite transition can be reduced by an increase of thermal conductivity with depth and a decrease of thermal expansivity with pressure (Matyska and Yuen, 2005; Tosi et al., 2010). In fact, increased radiative thermal conductivity can help to stabilize the chaotic situation in the D″ layer caused by exothermic post-perovskite transition (Matyska and Yuen, 2005).

The interaction of a cold descending slab with the D″ layer has always been an important dynamical problem. The piling up of slab material at the base of the mantle could play a role in the Earth's evolution. This topic becomes even more complex in the presence of post-perovskite. The possibility of slab material folding and piling at the base of the mantle and undergoing post-perovskite transition has been proposed by Hutko et al. (2006) based on strong lateral variations in seismic profiles. Lens-shaped post-perovskite structures, inferred from seismic imaging with ScS data (van der Hilst et al., 2007), have further attracted the attention of geodynamic modelers. Closely related issues of the seismologically observed complexity of the D″ layer include the relative effects of temperature and chemistry on the depth to and seismic visibility of the phase change and the distortion of the phase boundary by small-scale mantle convection.

Nakagawa and Tackley (2005, 2006) had carried out a series of models incorporating melting-induced chemical differentiation, platelike behavior, multiple phase transitions, and compressibility to focus on the interaction of slabs and the D″ layer for models with horizontal wavelengths longer than about 65 km. van den Berg et al. (2010a,b) had performed a combined geodynamic and seismological investigation for scale lengths as small as 4 km, including the presence of subducted MORB. They evaluated the seismic imaging manifestation of the heterogeneous distribution of mineral phase and composition in the model by subjecting the finite-element modeling results to a decomposition into wave packets (Duchkhov et al., 2010). The spatial scales and orientations (i.e., dips) are restricted to those that can be resolved by ScS imaging of large global network datasets (van der Hilst et al., 2007; Wang et al., 2006). The short-scale resolution is derived from a matrix representation of the generalized Radon transform, by exploiting the concentration of wave packets, and this approach opens new pathways for joint seismic and geodynamic analysis of a local region.

We show in **Figure 18** a zoom-in on the shear velocity variations of a post-perovskite lens structure of about 2000 km (top row), together with wave-packet decompositions at three different length scales. The wave speeds shown correspond to snapshots taken from thermal–chemical convection, the results having been converted from geodynamic output to seismic expressions by using mineral physics properties.

Three different scales $k = 4$–6, corresponding to length scales of around 12 km, are considered in this figure. The three bottom rows show results of an analysis zoomed in at the top of the post-perovskite lenses, displaying clearly the visibility of the corrugated top of the post-perovskite layer and a thicker bottom post-perovskite layer. A Clapeyron slope of 6 MPa K^{-1} is used in the simulation.

There is accumulating evidence that a strong viscosity contrast exists between perovskite and post-perovskite phases, with theoretical studies proposing a lower viscosity for post-perovskite (Ammann et al., 2010; Hunt et al., 2009). This is

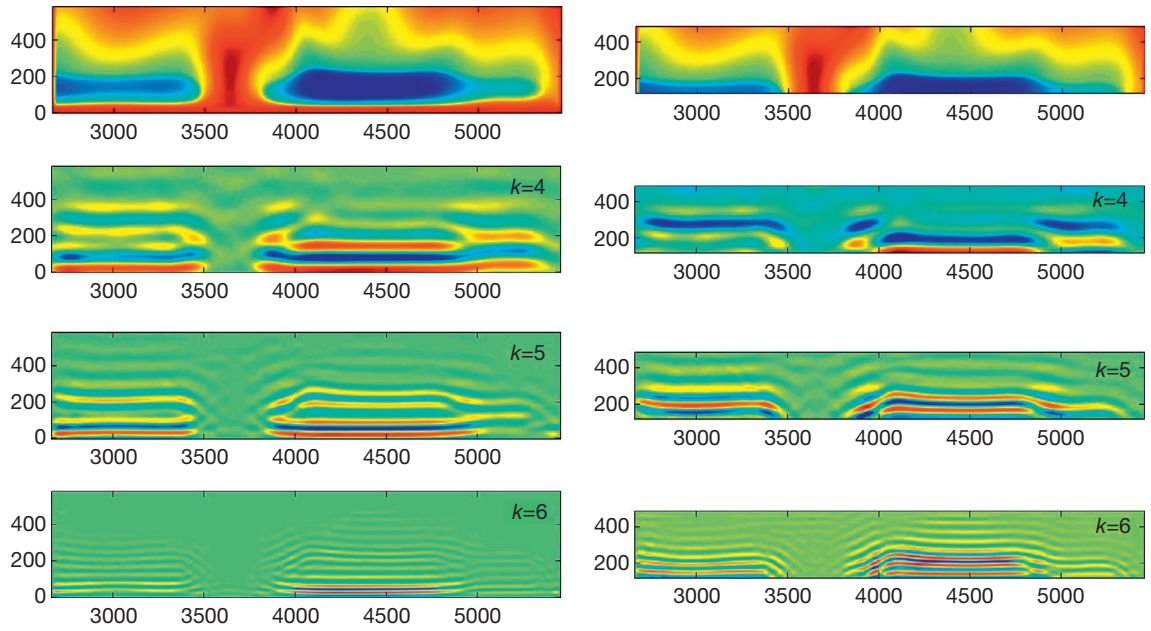

Figure 18 Wave-packet analysis for the observable character of shear-wave signatures obtained for a thermal–chemical convection with post-perovskite present. The model is two-dimensional and has a large aspect ratio (van den Berg et al., 2010a,b). We show here the seismic visibility of the lineaments of MORB crustal material in a background of pyrolitic material in the D″ region. The top row shows the variations in S-wave velocity. The second to bottom rows show the three wavenumber scales 4, 5, and 6 (van den Berg et al., 2010a), obtained from the wave-packet decomposition of the variations in shear-wave velocity. Left column, analysis of the bottom 600 km of the mantle; right column, results for a focused region showing the top of the post-perovskite lens.

supported by earlier inversions of intermediate-wavelength geoid anomalies and recent work based on the Earth's short-term rotational fluctuations (Cadek and Fleitout, 2006; Nakada and Karato, 2012; Tosi et al., 2009). Investigations focusing on this perovskite/post-perovskite rheological difference have found that the post-perovskite rheology can exert a noticeable influence on lower mantle dynamics and thermal evolution (Cizkova et al., 2010; Nakagawa and Tackley, 2011; Tosi et al., 2010), significantly amplifying the effects for post-perovskite assumed to have the same viscosity as perovskite.

Samuel and Tosi (2012) found that the presence of weak post-perovskite enhances heat transfer across the bottom thermal boundary layer, thus producing higher temperatures, reducing viscosities, and giving rise to considerably larger convective velocities. Small-scale fast convection is induced within the D″ layer and enhances local mixing. **Figure 19** shows the surface Nusselt number, which corresponds to the averaged surface heat flow and root-mean-squared velocity as a function of time for four different viscosity contrasts, ranging from ten times greater viscosity for post-perovskite to 0.01 lower viscosity for post-perovskite. There is a sharp reduction of the time scales when post-perovskite viscosity is decreased and a correspondingly rapid increase in the mean velocity. Mixing time was found to decrease dramatically with a 0.01 post-perovskite to perovskite viscosity ratio (Samuel and Tosi, 2012). With the development of post-perovskite in the secularly cooling deep mantle, the surface heat flow would increase dramatically that might cause a mantle overturn at 2.6 Byr ago (Breuer et al., 1996), manifested in a series of geologic and geobiological signatures (Maruyama et al., 2007). The time for the appearance of post-perovskite in the deep mantle is still uncertain but remains an important question in mantle evolution, especially in view of recent paper on the melting curve of pyrolite (Nomura et al., 2014), which found a lower melting temperature than previous results for pure $MgSiO_3$ minerals.

Mantle convection can be viewed dynamically as a nonlinear system (Bohr et al., 1998) because many thermodynamic parameters and transport properties such as thermal conductivity and viscosity depend sensitively on both temperature T and pressure P. The evolution of the Earth's mantle and core depends sensitively on the interactions among the various input parameters, such as the material properties and the time-varying boundary conditions. **Figure 20** shows a comparison of the dynamical time scales for the three different models, ranging from constant thermodynamic and thermal transport properties to variable thermodynamic parameters and thermal conductivity. The last case has a post-perovskite transition but with post-perovskite having the same viscosity as perovskite. Much faster time scales are present with constant properties, and the influences of variable thermal expansivity and the greater post-perovskite thermal conductivity are to greatly slow down the dynamics. In order to estimate the viscosity of the lower mantle from slab remnants inferred from seismic tomography (e.g., Li and Yuen, 2014; van der Meer et al., 2010), it is important to consider all physical parameters, such as thermal expansivity, conductivity, and chemical heterogeneities.

Figure 21 from Tosi et al. (2013) displays a comparison of the temperature fields for five different models. We show representative snapshots of selected simulations that were run until they reached a statistical steady state and the panels feature constant thermal expansivity α and conductivity k (**Figure 21(a)**), variable α and constant k (**Figure 21(b)**),

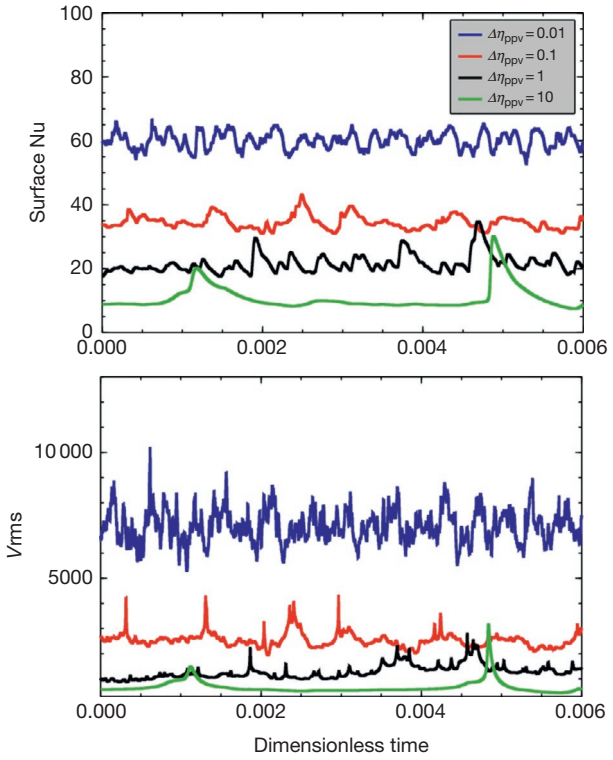

Figure 19 Influence of post-perovskite viscosity (η_{ppv}) on dynamical time scales. The averaged value of the surface heat flow and the root-mean-squared velocity of 2D mantle convection with post-perovskite are shown for various ratios of viscosity contrast between perovskite and post-perovskite, ranging from a stiffer post-perovskite to a much softer post-perovskite. In spite of the small volume occupied by post-perovskite in the mantle, the rheology of post-perovskite has strong influence on the time scales of the evolution of global mantle dynamics.

constant α and variable k (Figure 21(c) and 21(d)), and variable α and k (Figure 21(d) and 21(g)). Figure 21 shows temperature perturbations from the laterally averaged temperature profile. From Figure 21, it is quite evident that the influence of variable expansivity and conductivity on mantle convection is dramatic. When both parameters are held constant, the temperature field shows the character prevalent for convection at relatively high Rayleigh numbers with internal heating. The flow is dominated by cold downwellings, which, despite the viscosity jump between upper and lower mantle, sink straight to the CMB and accumulate there, cooling the deepest part of the mantle and producing the locally elevated post-perovskite lenses. Because of the limited temperature jump across the bottom thermal boundary layer, hot upwellings are generally weak and short-lived. In the presence of variable thermal conductivity, the mantle temperature increases sufficiently for plumes to be suppressed and post-perovskite forms only at places where cool downwellings reach the deep mantle. The distribution of thermal conductivity is dominated by pressure effects except in the core of cold slabs where it attains its highest values when temperature dependence is included. We emphasize here that despite their high conductivity, slabs do not heat up efficiently via conduction since they sink very rapidly because of the generally low viscosity of the surrounding hot mantle. The rapid sinking increases surface plate velocities. Using constant properties or just variable expansivity, plate velocities are in the range of a few cm a^{-1} or a fraction of cm a^{-1}, respectively. With variable conductivity, they can become up to one order of magnitude larger (e.g., the peak surface velocity associated with the slab of Figure 21(f) is around 30 cm a^{-1}). The differences between models featuring P-dependent and P- and T-dependent k are minor, both qualitatively (compare Figure 21(c) and 21(d)) and quantitatively. In terms of temperature distribution, the largest differences are attained in the lower mantle and amount to 0.02 (74 K).

When both variable α and k are considered together (Figure 21(d) and 21(g)), we find another convective regime. Because of the temperature increase caused by the elevated thermal conductivity at depth and the modified buoyancy properties induced by variations of thermal expansivity, both up- and downwellings assume equal importance. In particular, whether we use either A or B models, convection shows an increased propensity toward local layering, with slabs that are often trapped in the transition zone before sinking into the lower mantle where the associated cold thermal anomaly also tends to broaden. Occasionally, slab detachment caused by a period of prolonged stagnation can also be observed, as shown in Figure 21(g). Furthermore, the slowing effect exerted by variable expansivity helps to reduce high surface velocities to more realistic plate values from ~4 to 5 cm a^{-1}.

Self-consistent mineral physics within a thermodynamic framework (Connolly, 2005) has been employed by Nakagawa et al. (2010, 2012) to study the influence of oceanic crust on thermal–chemical mantle convection with post-perovskite transition. Models were originally run for 3D geometry (Nakagawa et al., 2010), but to obtain proper resolution, a more modest spherical annulus geometry (Nakagawa et al., 2012) was employed in order to resolve the CMB region at 10 km radial resolution and has 30 tracers per cell to track accurately the composition and melt fraction. In Figure 22, we show their results for temperature, composition, and seismic perturbations in bulk sound velocity and shear waves at a time of 4.5 Gyr from the beginning and for bulk composition of MORB and harzburgite and pyrolite taken from Ringwood (1985). We can see that the cold subducted slabs are deformed greatly in the deep mantle and have a tendency to produce folded structures above the CMB (Hutko et al., 2006). The basaltic crust is separated from subducted slabs above the CMB and then piles up to form large-scale compositionally distinct structures. Upwelling plumes are observed to rise from the edge of the basaltic piles or between the pooled cold regions. In the shear velocity field, post-perovskite increases the velocity contrast between the piles and the cold pool between the piles. On the other hand, post-perovskite reverses the sign of the bulk sound velocity contrast, making the cold region slower than the piles. This causes the correlation between the shear and bulk sound velocities to be small or negative in the bottom part of the mantle and positive above this region. These results indicate that both mineral physics together with geodynamics must be employed together to unravel the complicated structures in the D″ layer, which come from the dynamics of the slab interacting with the D″ layer and the delicate balance among thermal, phase, and compositional influences on seismic structure.

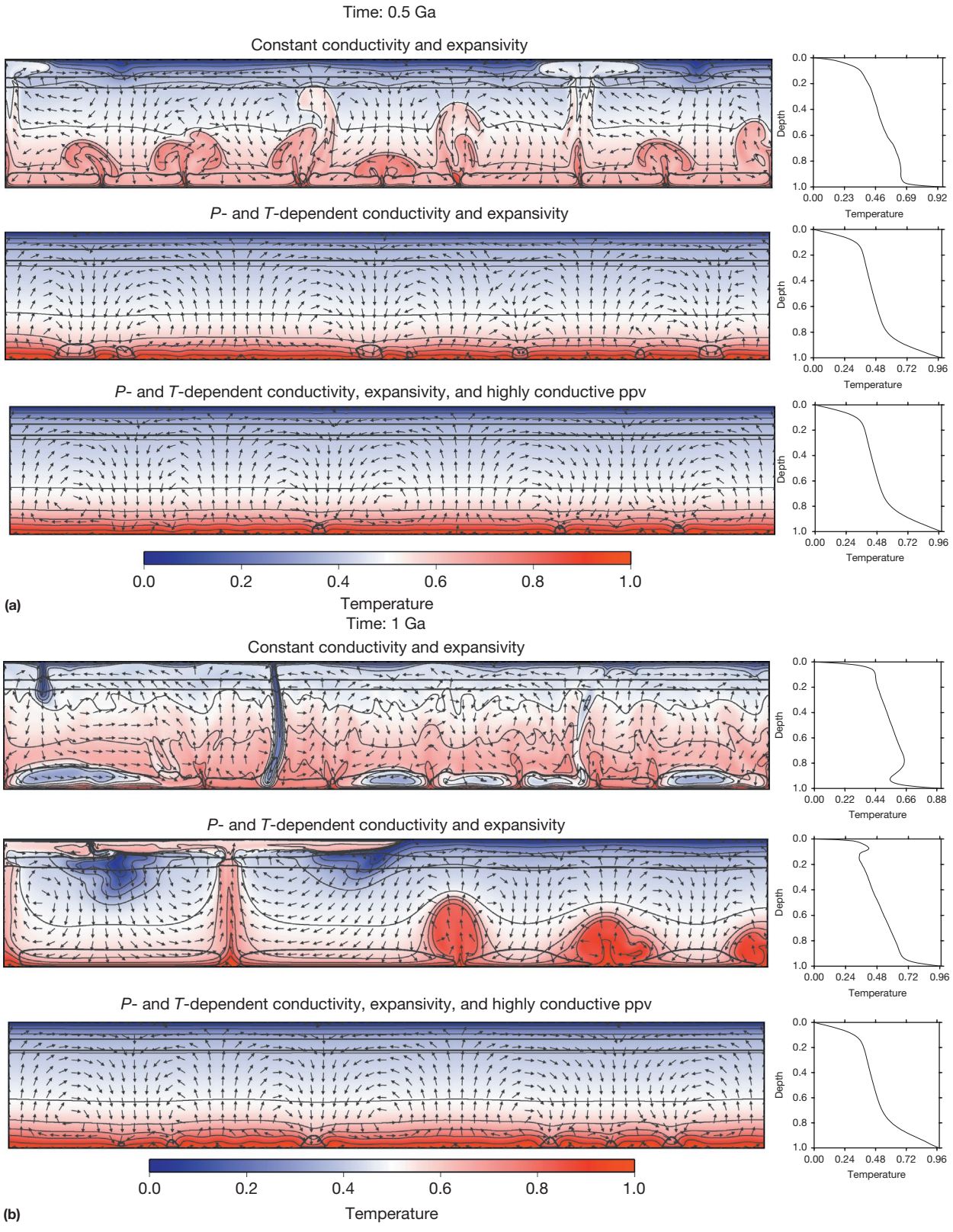

Figure 20 (Continued)

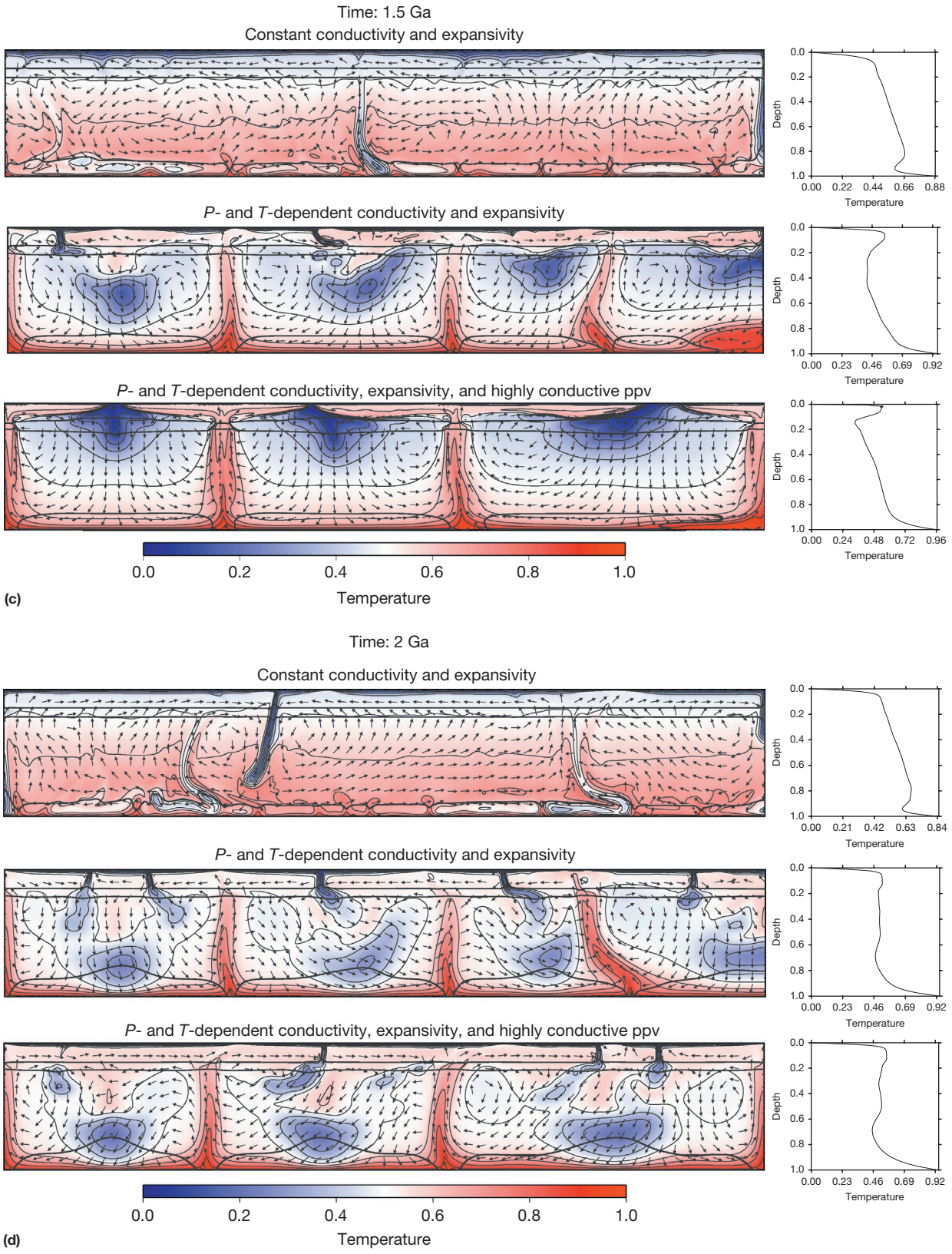

Figure 20 Comparison of the dynamical scales among models with constant thermal conductivity and conductivity, temperature- and pressure-dependent thermal conductivity and expansivity, and temperature- and pressure-dependent thermal conductivity and expansivity in addition to a highly conductive post-perovskite (e.g., Ohta et al., 2012a,b). Both the spinel to perovskite and perovskite to post-perovskite transitions are included in all models. The rheology is temperature- and pressure-dependent (Tosi et al., 2013). We note that the time scales are fastest for the constant thermal conductive and expansivity model and slowest when the more conductive post-perovskite is employed.

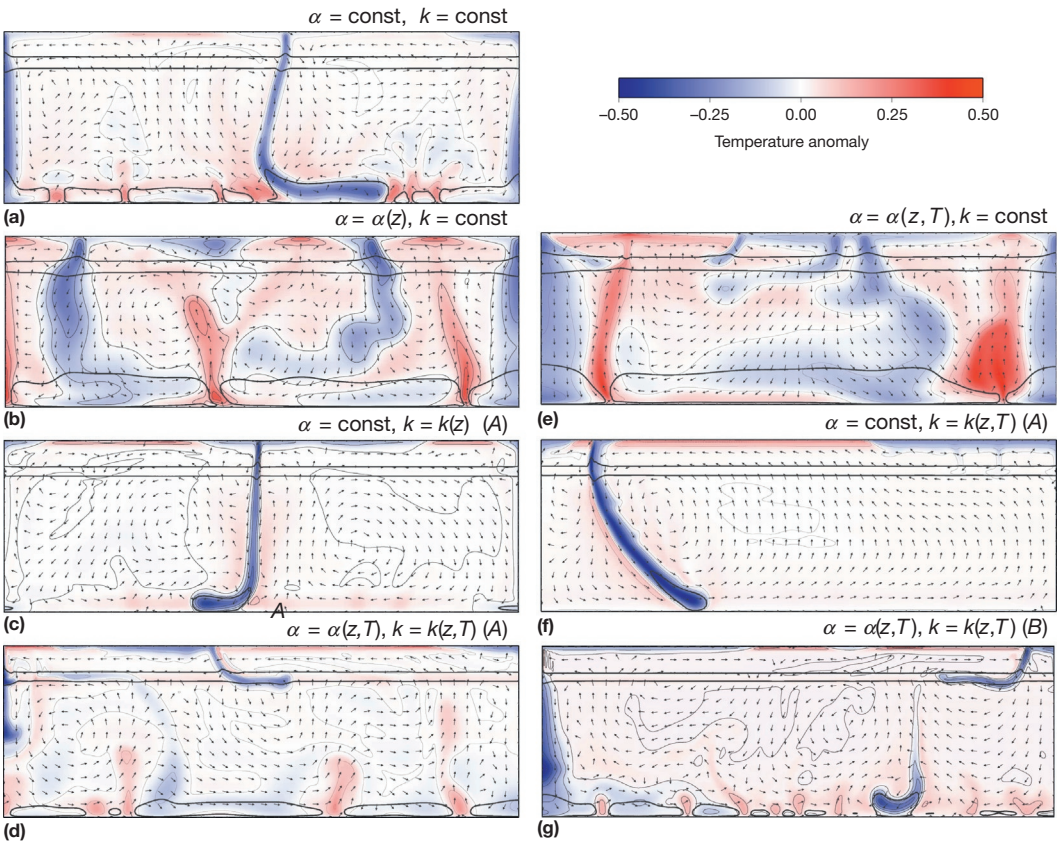

Figure 21 A comparison of the temperature anomaly fields and velocity vectors for seven different models. Models feature constant thermal expansivity and thermal conductivity (panel a), variable thermal expansivity and constant thermal conductivity (panels b and e), constant thermal expansivity and variable thermal conductivity (panels c and f), and both variable thermal conductivity and expansivity (panels d and g). Arrow indicates the direction of the flow field. Two different depth-dependent thermal conductivity models (A and B) have been considered. Reproduced from Tosi N, Yuen D, de Koker N, and Wentzcovitch RM (2013) Mantle dynamics with pressure- and temperature-dependent thermal expansivity and conductivity. *Physics of the Earth and Planetary Interiors* 217: 48–58, http://dx.doi.org/10.1016/j.pepi.2013.02.004.

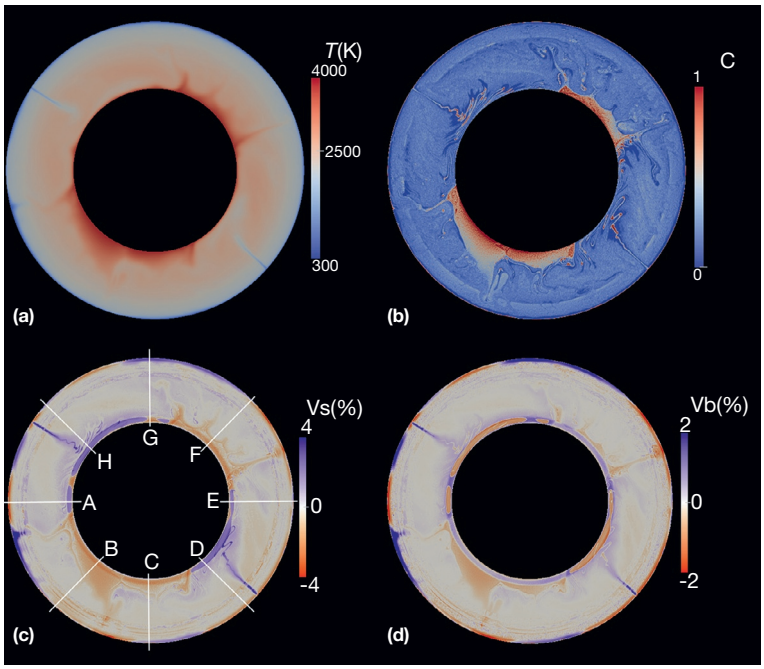

Figure 22 Temperature, composition, shear velocity, and bulk sound velocity from high-resolution two-dimensional convection in a spherical annulus. Snapshots are taken at 4.5 Ga from the beginning of the simulation (Nakagawa et al., 2012). The thermodynamic approach to mineral physics from Connolly (2005) has been employed to calculate the seismic expressions from convection simulation.

2.05.5.2 Heat Flux Constraints

Assuming that the D″ seismic discontinuity is a manifestation of the post-perovskite phase transition, temperature in the lowermost mantle can be estimated from the phase diagram for an assumed composition and mineral assemblage. Moreover, a shear-wave velocity reduction observed below the D″ discontinuity may be caused by back-transformation from post-perovskite to perovskite due to rapid increase in temperature in the thermal boundary layer above the CMB. This 'double-crossing' scenario (the lowermost mantle geotherm intersects the phase boundary twice) was originally proposed by Hernlund et al. (2005) and can be used to constrain the temperature gradient in D″ and, for a given choice of thermal conductivity, the associated heat flow (e.g., Hernlund et al., 2005; Lay et al., 2006; van der Hilst et al., 2007).

Nomura et al. (2014) had found that the solidus temperature of pyrolite can be some five hundred degrees lower than the melting temperature for perovskite mineral (Boehler, 1996). This result has important implications for the amount of post-perovskite in the lower mantle and the amount of coverage of post-perovskite over the global CMB surface. **Figure 23** displays the coverage of post-perovskite (gray color) over the CMB surface. This snapshot was taken from numerical simulations in 3D spherical convection using very high-resolution and statistical techniques for quantifying the relationships of depths of double-crossings of the post-perovskite transition developed in 3D convection (Monnereau and Yuen, 2010). The global coverage over the CMB surface by post-perovskite today is an important factor in the overall heat flux as a function of mantle evolution and should be a probed with detailed seismic arrays because from the estimate of this quantity, we can derive better constraint on the timing of post-perovskite appearance in the lower mantle.

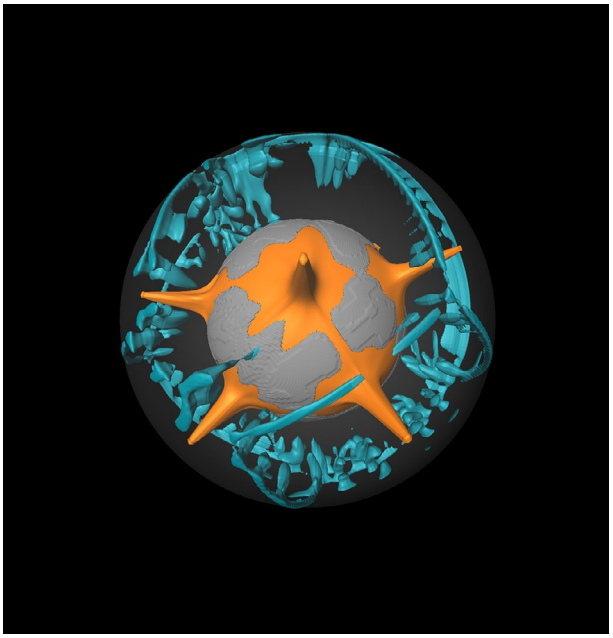

Figure 23 Snapshot of 3D spherical convection showing the coverage of post-perovskite (gray color) over the core–mantle boundary surface. Blue and orange colors denote cold and hot material, respectively. Calculations are taken from Monnereau and Yuen (2007, 2010), in which both thermal conductivity and thermal expansivity are depth-dependent. The viscosity is depth-dependent with a jump at 670 km depth. Three mantle phase transitions are included.

2.05.5.3 Dynamical Effects of Post-Perovskite in Other Planets

The interiors of exosolar planets (Marcy and Butler, 1995) represent a new fertile field for planetary scientists and astronomers to research together. Most such planets found up to now are much larger than the Earth, typically the size of Jupiter. But recently, several planets, dubbed super-Earths, have been detected near the star Gliese 876, with estimates of about seven Earth masses. A nearby star Gliese 581 hosts several more of these large planets, with some being rocky. The mantles of these rocky planetary interiors represent a frontier area for mineral physics and dynamical modelers, as post-perovskite will play an important role. The mineralogy of super-Earth interiors will undergo additional structural changes at extreme (TPa) pressures (Coppari et al., 2013; Umemoto et al., 2006b). Geodynamicists have begun to model the mantle dynamics of exosolar planets (O'Neill and Lenardic, 2007; Tackley et al., 2013; Valencia et al., 2007a,b,c) but very few have included the influences of phase transitions, in particular the perovskite-to-post-perovskite transition and the higher pressure decomposition of post-perovskite (Umemoto et al., 2006b).

van den Berg et al. (2010b) modeled the time-dependent dynamics of exosolar planets within the framework of a two-dimensional Cartesian model and the extended Boussinesq approximation and included the post-perovskite transition and its deeper decomposition to the oxides (Umemoto et al., 2006a). The mass of the super-Earth models considered is eight times the Earth's mass and the thickness of the mantle is 4,700 km. The effects of depth-dependent properties have been considered for the thermal expansion coefficient, the viscosity, and thermal conductivity. The viscosity and thermal conductivity are also temperature-dependent. The thermal conductivity has contributions from phonons, photons, and electrons. The last dependence comes from the bandgap nature of the material under high pressure and increases exponentially with temperature and kicks in at temperatures above 5,000 K. The thermal expansivity decreases by a factor of 20 across the mantle because of the high pressure, greater than 1 TPa. They considered three phase transitions: the spinel to perovskite, the post-perovskite, and the post–post-perovskite decomposition in the deep lower mantle, for which the Clapeyron slope is strongly negative -18 MPa K^{-1} (Umemoto et al, 2006a), inducing layered convection in the deep portion of the exoplanet.

Their results show that because of the multiple phase transitions and strongly depth-dependent properties, particularly the thermal expansion coefficient, most of the planetary interior is strongly superadiabatic initially in spite of a high surface Rayleigh number, because of the presence of partially layered and penetrative convective flows throughout the mantle, unlike convection in the Earth's mantle. This period of superadiabaticity can last a very long time, more than a couple of Ga. An outstanding influence of electronic thermal conductivity is to heat up the bottom boundary layer quasi-periodically, giving rise to strong coherent superplumes, which can punch their way to the upper mantle and break up the layered convective

pattern and may give rise to planetary-scale super volcanism. Figure 24 displays representative snapshots of the temperature field and corresponding stream functions for three model cases all with the negative Clapeyron slope, with the same temperature contrast $\Delta T = 10\,000$ K.

The only difference in the models is the thermal conductivity, with models A and B having constant conductivity, while model C has contributions from phonons, photons, and electrons. The last component has an exponential dependence in T. The different degree in the style of layered convection near the bottom post–post-perovskite decomposition boundary can be clearly discerned in these frames, in particular in the distribution and spacing of the contour lines in the stream function. Model A with a decrease factor of thermal expansivity across the mantle of 0.1 shows limited interaction between the endothermic phase boundaries, with hot plumes crossing the phase boundary in several locations. The middle row of snapshots for model B with thermal expansivity contrast of 0.05 illustrates that a penetrative convective flow regime in the stream function with flow fields concentrated in the top half of the mantle and the bottom circulation is driven by the convection cells in the shallow mantle. As in the A model, the flow is driven by the cold downwellings. The temperature snapshots reveal an increased layering at the post–post-perovskite boundary at the bottom, as indicated by the mushroom-shaped plumes, which show only limited penetration of the deepest phase boundary. The increase in layering between models A and B is related to the smaller value of the thermal expansivity near the bottom post-perovskite decomposition resulting in a higher effective phase buoyancy parameter that scales inversely with respect to thermal expansion coefficient (Christensen and Yuen, 1985). A similar type of layered penetrative convection was observed in Breuer et al. (1997) in a model for the Martian mantle.

In contrast to the constant thermal conductivity models, model C has a variable thermal conductivity $k(T,P)$ model with a strong contribution from electron thermal conductivity k_{el} near the bottom of the mantle, where temperatures are in excess of 5,000 K. The high conductivity at the base of the mantle results in an increased heat flow into the bottom post-perovskite decomposition layer, producing episodic occurrence of massive mantle plumes that break through the phase boundary, as illustrated by the hot plume near the middle of the temperature frame and corresponding high vertical velocity shown by the very narrow spacing in the stream functions. These events may trigger volcanism on the surface of exoplanets, which may be detectable someday by space telescope (Kaltenegger et al., 2011). We depict this scenario in Figure 25.

The viscosity of the post-perovskite lower mantle in exosolar planet has attracted the attention of mantle rheologists, and there is currently a debate between computational mineral physicists (Ammann et al., 2010), who argued from dislocation theory and experimental rheologists (Karato, 2011, 2013), who relied on ideas from diffusion of vacancies. Ito and Toriumi (2007) had shown from large-scale MD simulations of MgO that a viscosity maximum can be found under high enough pressure. Using high-resolution boundary-element method simulations, Morra et al. (2010) had found that pulsating plumes can also be developed by a Rayleigh–Taylor type of instability from these types of viscosity 'hills' in the Earth's

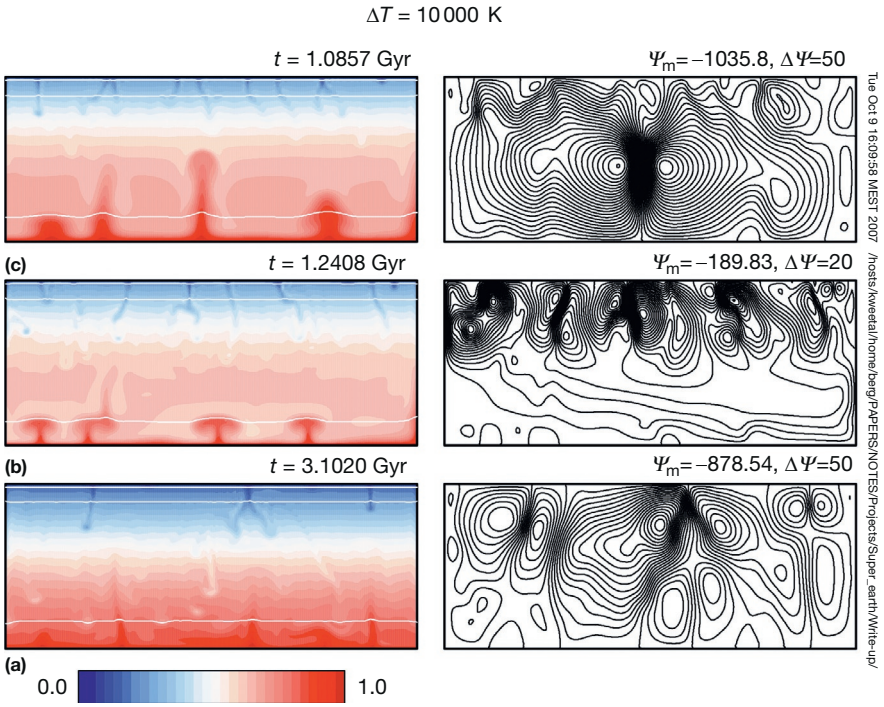

Figure 24 Temperature and stream functions associated high-resolution two-dimensional simulations of convection in an exoplanet. Three different models have been considered in these time-dependent runs (van den Berg et al., 2010a,b). A temperature contrast of 10000° across the exoplanet with a mass eight times that of the Earth has been assumed. Decomposition of post-perovskite at ultrahigh pressures close to 1 Tpa (Umemoto et al., 2006a) has been employed with a strong negative Clapeyron slope of -18 MPa K^{-1}. The thermal conductivity model has contributions from phonons, photons, and electrons. Rheology is only temperature-dependent with a lateral contrast of 10000.

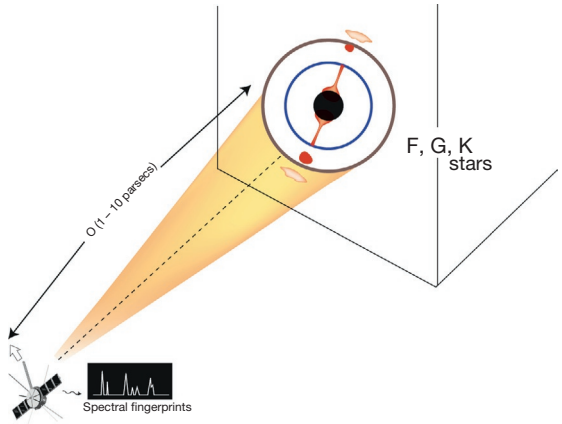

Figure 25 Possible future scenario of space telescopic detection of volcanic gas (Kaltenegger et al., 2011) coming from pulsating plumes in exosolar planets due to the interaction (Morra et al., 2010) between an upwelling and a viscosity hill predicted by the work of Ito and Toriumi (2007) and Karato (2011, 2013).

mantle. Karato (2011, 2013) had developed a new idea of viscosity maximum in the post-perovskite mantle, which is followed below by a low-viscosity deep mantle in large exosolar planets. The style of exoplanetary convection between the two rheological models (Ammann et al., 2010; Karato, 2011) may be tested by searching for spectral fingerprints from emitted volcanic gases (see **Figure 24**), where we would expect to more volcanic gases to be emitted by the plume pulsation model.

2.05.5 Conclusions

The extensive investigations of the post-perovskite phase described here represent a major advance in our understanding of deep mantle mineralogy, transport properties, and dynamics. Given the predominance of silicate perovskite in the lower mantle, the importance of discovery and characterization of post-perovskite brought multidisciplinary focus on this new phase. Many questions remain about post-perovskite in the Earth and in other planets, and the breadth of investigations will continue for much time to come, ultimately modifying some of the findings reported in this summary.

Acknowledgments

Our research on post-perovskite has been supported by NSF/ITR 0428774, NSF/EAR 1019853 (R.M.W. and D.A.Y.), and NSF/EAR 1341862 (R.M.W.) and NSF Grant EAR-1245717 (T.L.).

References

Akahama Y, Kawamura H, and Singh AK (2002) Equation of state of bismuth to 222 GPa and comparison of gold and platinum pressure scales to 145 GPa. *Journal of Applied Physics* 92: 5892–5897.

Akber-Knutson S, Steinle-Neumann G, and Asimow PD (2005) Effect of Al on the sharpness of the $MgSiO_3$ perovskite to post-perovskite phase transition. *Geophysical Research Letters* 32: L14303. http://dx.doi.org/10.1029/2005GL023192.

Allegre CJ (1997) Limitations on the mass exchange between the upper- and lower-mantle: The evolving convective regime of the Earth. *Earth and Planetary Science Letters* 150: 1–6.

Allègre CJ, Poirier J-P, Humler E, and Hofmann AW (1995) The chemical composition of the Earth. *Earth and Planetary Science Letters* 185: 49–69.

Ammann MW, Brodholt JP, Wookey J, and Dobson DP (2010) First-principles constraints on diffusion in lower-mantle minerals and a weak D″ layer. *Nature* 465: 462–465. http://dx.doi.org/10.1038/nature09052.

Anderson OL, Isaak DG, and Yamamoto S (1989) Anharmonicity and the equation of state for gold. *Journal of Applied Physics* 65: 1534–1543.

Andrault D (2001) Evaluation of (Mg, Fe) partitioning between silicate perovskite and magnesiowüstite up to 120 GPa and 2300 K. *Journal of Geophysical Research* 106: 2079–2087.

Andrault D, Muñoz M, Bolfan-Casanova N, et al. (2010) Experimental evidence for perovskite and post-perovskite coexistence throughout the whole D″ region. *Earth and Planetary Science Letters* 293: 90–96.

Badro J, Fiquet G, Guyot F, et al. (2003) Iron partitioning in Earth's mantle: Toward a deep lower mantle discontinuity. *Science* 300: 789–791.

Badro J, Rueff JP, Vankó G, et al. (2004) Electronic transitions in perovskite: Possible nonconvecting layers in the lower mantle. *Science* 305: 383–386.

Belonoshko A, Skorodumova NV, Rosengren A, et al. (2005) High-pressure melting of $MgSiO_3$. *Physical Review Letters* 94: 195701.

Boehler R (1996) Melting temperature of the Earth's mantle and core: Earth's thermal structure. *Annual Reviews of Earth and Planetary Sciences* 24: 15–40.

Bohr T, Jensen MH, Paladin G, and Vulpiani A (1998) *Dynamical Systems Approach to Turbulence*. Cambridge, UK: Cambridge University Press, 377 pp.

Boyet M and Carlson RW (2005) ^{142}Nd evidence for early (>4.53 Ga) global differentiation of the silicate Earth. *Science* 309: 576–581.

Breuer D, Yuen DA, and Spohn T (1997) Phase transitions in the Martian mantle: Implications for partially layered convection. *Earth and Planetary Science Letters* 148: 457–469.

Breuer D, Zhou H, Yuen DA, and Spohn T (1996) Phase transition in the Martian mantle, implications for the planet's volcanic history. *Journal of Geophysical Research* 101(E3): 7531–7542.

Brown MJ and Shankland TJ (1981) Thermodynamic parameters in the Earth as determined from seismic profiles. *Geophysical Journal Royal Astronomical Society* 66: 579–596.

Buffett BA, Garnero EJ, and Jeanloz R (2000) Sediments at the top of Earth's core. *Science* 290: 1338–1342.

Cadek O and Fleitout LM (2006) Effects of lateral viscosity variations in D″ on predictions of the long-wavelength geoid. *Studia Geophysica et Geodaetica* 50: 217–232.

Caracas R and Cohen RE (2005) Effect of chemistry on the stability and elasticity of the perovskite and post-perovskite phases in the $MgSiO_3$–$FeSiO_3$–Al_2O_3 system and implications for the lowermost mantle. *Geophysical Research Letters* 32: L16310. http://dx.doi.org/10.1029/2005GL023164.

Carrier P, Wentzcovitch RM, and Tsuchiya J (2007) First principles prediction of crystal structures at high temperatures using the quasiharmonic approximation. *Physics Review B* 76: 064116.

Catalli K, Shim SH, and Prakapenka V (2009) Thickness and Clapeyron slope of the post-perovskite boundary. *Nature* 462: 782–785.

Christensen UR and Yuen DA (1984) The interaction of a subducting lithospheric slab with a chemical or phase boundary. *Journal of Geophysical Research* 89(B6): 4389–4402.

Christensen UR and Yuen DA (1985) Layered convection induced by phase transitions. *Journal of Geophysical Research* 90(B12): 10291–10300.

Cizkova H, Cadek O, Matyska C, and Yuen DA (2010) Implications of post-perovskite transport properties for core–mantle dynamics. *Physics of Earth and Planetary Interiors* 180: 235–243.

Connolly JAD (2005) Computation of phase equilibria by linear programming: A tool for geodynamical modeling and its application to subduction zone decarbonation. *Earth and Planetary Science Letters* 236: 524–541.

Coppari F, Smith RF, Eggert JH, et al. (2013) Experimental evidence for a phase transition in magnesium oxide at exoplanet pressures. *Nature Geoscience* 6: 926–929.

da Silva CRS, Wentzcovitch RM, Patel A, Price GD, and Karato S-I (2000) The composition and geotherm of the lower mantle: Constraints from the calculated elasticity of silicate perovskite. *Physics of Earth and Planetary Interiors* 118: 103.

de Koker N, Steinle-Neumann G, and Vlček V (2012) Electrical resistivity and thermal conductivity of liquid Fe alloys at high P and T, and heat flux in Earth's core. *Proceedings of the National Academy of Sciences of the United States of America* 190: 4070–4073.

Dekura H, Tsuchiya T, and Tsuchiya J (2013) Ab initio lattice thermal conductivity of $MgSiO_3$ perovskite as found in Earth's lower mantle. *Physical Review Letters* 110: 025904.

Dobson DP and Brodholt JP (2000) The electrical conductivity and thermal profile of the earth's mid-mantle. *Geophysical Research Letters* 27: 2325–2328.

Dobson DP and Brodholt JP (2005) Subducted banded iron formations as a source of ultralow-velocity zones at the core–mantle boundary. *Nature* 434: 371–374.

Dorfman SM, Shieh SR, Meng Y, Prakapenka VB, and Duffy TS (2012) Synthesis and equation of state of perovskites in the $(Mg, Fe)_3Al_2Si_3O_{12}$ system to 177 GPa. *Earth and Planetary Science Letters* 357–358: 194–202.

Dorogokupets PI and Dewaele A (2007) Equations of state of MgO, Au, Pt, NaCl-B1, and NaCl-B2: Internally consistent high-temperature pressure scales. *High Pressure Research* 27: 431–446.

Duchkov AA, Andersson F, and deHoop MV (2010) Discrete, almost symmetric wave packets and multiscale geometrical representation of (seismic) waves. *IEEE Geosciences and Remote Sensing Transactions* 48(9): 3408–3423.

Dziewonski AM and Anderson DL (1981) Preliminary reference Earth model. *Physics of the Earth and Planetary Interiors* 25: 297–356.

Fei Y, Orman JV, Li J, et al. (2004) Experimentally determined postspinel transformation boundary in Mg_2SiO_4 using MgO as an internal pressure standard and its geophysical implications. *Journal of Geophysical Research* 109: B02305. http://dx.doi.org/10.1029/2003JB002562.

Fei Y, Ricolleau A, Frank M, Mibe K, Shen G, and Prakapenka V (2007) Toward an internally consistent pressure scale. *Proceedings of the National Academy of Sciences of the United States of America* 104: 9182–9186.

Fiquet G, Dewaele A, Andrault D, Kunz M, and Bihan TL (2000) Thermoelastic properties and crystal structure of $MgSiO_3$ perovskite at lower mantle pressure and temperature conditions. *Geophysical Research Letters* 27: 21–24. http://dx.doi.org/10.1029/1999GL008397.

Forte AM, Woodward RL, and Dziewonski AM (1994) Joint inversions of seismic and geodynamic data for models of 3-dimensional mantle heterogeneity. *Journal of Geophysical Research* 99: 21857–21878.

Frost DJ, Asahara Y, Rubie DC, et al. (2010) Partitioning of oxygen between the Earth's mantle and core. *Journal of Geophysical Research* 115: B02202. http://dx.doi.org/10.1029/2009JB006302.

Garnero E (2004) A new paradigm for Earth's core–mantle boundary. *Science* 304: 834–836.

Garnero E, Maupin V, Lay T, and Fouch MJ (2004) Variable azimuthal anisotropy in Earth's lowermost mantle. *Science* 306: 259–261.

Goncharov AF, Haugen BD, Struzhkin VV, Beck P, and Jacobsen SD (2008) Radiative conductivity in the Earth's lower mantle. *Nature* 456: 231–234.

Grocholski B, Catalli K, Shim S-H, and Prakapenka V (2012) Mineralogical effects on the detectability of the postperovskite boundary. *Proceedings of the National Academy of Sciences of the United States of America* 109: 2275–2279.

Haigis V, Salanne M, and Jahn S (2012) Thermal conductivity of MgO, $MgSiO_3$ perovskite and post-perovskite in the Earth's deep mantle. *Earth and Planetary Science Letters* 355–356: 102–108.

Harder H and Christensen UR (1996) A one-plume model of Martian mantle convection. *Nature* 380: 507–509.

Hernlund JW, Thomas C, and Tackley PJ (2005) A doubling of the postperovskite phase boundary and structure of the Earth's lower mantle. *Nature* 434: 882–884.

Hirose K (2002) Phase transitions in pyrolitic mantle around 670-km depth: Implications for upwelling of plumes from the lower mantle. *Journal of Geophysical Research* 107. http://dx.doi.org/10.1029/2001JB000597.

Hirose K (2007) Discovery of post-perovskite phase transition and the nature of D″ layer In: Hirose K, Brodholt J, Lay T, and Yuen DA (eds.) *Post-Perovskite: The Last Mantle Phase Transition*, pp. 19–35. Washington, DC: American Geophysical Union.

Hirose K and Fujita Y (2005) Clapeyron slope of the post-perovskite phase transition boundary in $CaIrO_3$. *Geophysical Research Letters* 32: L13313. http://dx.doi.org/10.1029/2005GL023219.

Hirose K, Karato S, Cormier V, Brodholt J, and Yuen D (2006) Unsolved problems in the lowermost mantle. *Geophysical Research Letters* 33: L12S01. http://dx.doi.org/10.1029/2006GL025691.

Hirose K and Kawamura K (2007) Discovery of post-perovskite phase transition and implications for the nature of D″ layer of the mantle In: Ohtani E (ed.) *Advances in High-Pressure Mineralogy*, 421, pp. 37–46. http://dx.doi.org/10.1130/2007.2421(03). Geol. Soc. Ame. Special Paper.

Hirose K, Kawamura K, Ohishi Y, Tateno S, and Sata N (2005) Stability and equation of state of $MgGeO_3$ post-perovskite phase. *American Mineralogist* 90: 262–265.

Hirose K, Nagaya Y, Merkel S, and Ohishi Y (2010) Deformation of MnGeO3 post-perovskite at lower mantle pressure and temperature. *Geophysical Research Letters* 37: L20302. http://dx.doi.org/10.1029/2010GL044977.

Hirose K, Sata N, Komabayashi T, and Ohishi Y (2008) Simultaneous volume measurements of Au and MgO to 140 GPa and thermal equation of state of Au based on the MgO pressure scale. *Physics of the Earth and Planetary Interiors* 167: 149–154.

Hirose K, Sinmyo R, Sata N, and Ohishi Y (2006) Determination of post-perovskite phase transition boundary in $MgSiO_3$ using Au and MgO internal pressure standards. *Geophysical Research Letters* 33: L01310. http://dx.doi.org/10.1029/2005GL024468.

Hirose K, Takafuji N, Fujino K, Shieh SR, and Duffy TS (2008) Iron partitioning between perovskite and post-perovskite: A transmission electron microscope study. *American Mineralogist* 93: 1678–1681. http://dx.doi.org/10.2138/am.2008.3001.

Hirose K, Takafuji N, Sata N, and Ohishi Y (2005) Phase transition and density of subducted MORB crust in the lower mantle. *Earth and Planetary Science Letters* 237: 239–251.

Hohenberg P and Kohn W (1964) Inhomogeneous electron gas. *Physical Review* 136: B864–B871.

Holme R (1998) Electromagnetic core–mantle coupling: II. Probing deep mantle conductance. In: Gurnis M, Wysession ME, Knittle E, and Buffett BA (eds.) *The Core–Mantle Boundary Region*, pp. 139–151. Washington, DC: American Geophysical Union.

Holmes NC, Moriarty JA, Gathers GR, and Nellis WJ (1989) The equation of state of platinum to 660 GPa (6.6 MBar). *Journal of Applied Physics* 66: 2962–2967.

Honda S, Yuen DA, Balachandar S, and Reuteler DM (1993) Three-dimensional instabilities of mantle convection with multiple phase transitions. *Science* 259: 1308–1311.

Howard AW, Marcy GW, Johnson JA, et al. (2010) The occurrence and mass distribution of close-in super-Earths, Neptunes, and Jupiters. *Science* 330: 653–655.

Humayun M, Qin L, and Norman MD (2004) Geochemical evidence for excess iron in the mantle beneath Hawaii. *Science* 306: 91–94.

Hunt SA, Davie DR, Walker AM, et al. (2012) On the increase in thermal diffusivity caused by the perovskite to post-perovskite phase transition and its implications for mantle dynamics. *Earth and Planetary Science Letters* 319–320: 96–103.

Hunt SA, Weidner DJ, Li L, et al. (2009) Weakening of calcium iridate during its transformation from perovskite to post-perovskite. *Nature Geosciences* 2: 794–797.

Hutko A, Lay T, Garnero EJ, and Revenaugh JS (2006) Seismic detection of folded, subducted lithosphere at the core–mantle boundary. *Nature* 441: 333–336.

Hutko AR, Lay T, and Revenaugh J (2009) Localized double-array stacking analysis of PcP: D″ and ULVZ structure beneath the Cocos Plate, Mexico, central Pacific and north Pacific *Physics of the Earth and Planetary Interiors* 173: 60–74.

Hutko A, Lay T, Revenaugh J, and Garnero EJ (2008) Anticorrelated seismic velocity anomalies from post-perovskite in the lowermost mantle. *Science* 320: 1070–1074.

Iitaka T, Hirose K, Kawamura K, and Murakami M (2004) The elasticity of the $MgSiO_3$ post-perovskite phase in the Earth's lowermost mantle. *Nature* 430: 442–445.

Irifune T (1994) Absence of an aluminous phase in the upper part of the lower mantle. *Nature* 370: 131–133.

Irifune T, Higo Y, Inoue T, Kono Y, Ohfuji H, and Funakoshi K (2008) Sound velocities of majorite garnet and the composition of the mantle transition region. *Nature* 451: 814–817.

Irifune T, Nishiyama N, Kuroda K, et al. (1998) The post-spinel phase boundary in Mg_2SiO_4 determined by in-situ X-ray diffraction. *Science* 279: 1698–1700.

Irifune T, Shinmei T, McCammon CA, Miyajima N, Rubie DC, and Frost DJ (2010) Iron partitioning and density changes of pyrolite in Earth's lower mantle. *Science* 327: 193–195.

Ishii M and Tromp J (1999) Normal-mode and free-air gravity constraints on lateral variations in velocity and density of Earth's mantle. *Science* 285: 1231–1236.

Ito Y and Toriumi M (2007) Pressure effects of self-diffusion in periclase (MgO) by molecular dynamics. *Journal of Geophysical Research* 112: B4. http://dx.doi.org/10.1029/2005.JB003685.

Jamieson JC, Fritz JN, and Manghnani MH (1982) Pressure measurement at high temperature in x-ray diffraction studies: Gold as a primary standard. In: Akimoto S, et al. (ed.) *High-Pressure Research in Geophysics*, pp. 27–48. Tokyo: CAPJ.

Jones GM (1977) Thermal interaction of the core and mantle and long-term behavior of the geomagnetic fields. *Journal of Geophysical Research* 82: 1703–1709.

Kaltenegger L, Segura A, and Mohanty S (2011) Characterizing model spectra of the first habitable Super-Earth-Gl581d. *The Astrophysical Journal* 733: 1–12.

Karato S (2011) Rheological structure of the mantle of a super-Earth: Some insights from mineral physics. *Icarus* 212: 14–23.

Karato S (2013) Rheological properties of minerals and rocks. In: Karato S (ed.) *Physics and Chemistry of the Deep Earth*. Chichester: Wiley-Blackwell.

Karato S and Karki BB (2001) Origin of lateral variation of seismic wave velocities and density in the deep mantle. *Journal of Geophysical Research* 106: 21771–21783.

Karki BB, Stixrude L, and Crain J (1997) Ab initio elasticity of the three high-pressure polymorphs of silica. *Geophysical Research Letters* 24: 3269–3272.

Karki BB, Wentzcovitch RM, de Gironcoli S, and Baroni S (2000) Ab initio lattice dynamics of $MgSiO_3$-perovskite. *Physical Review* B1(62): 14750–14756.

Karki BB, Wentzcovitch RM, de Gironcoli S, and Baroni S (2001) First principles thermoelasticity of $MgSiO_3$-perovskite: Consequences for the inferred properties of the lower mantle. *Geophysical Research Letters* 28: 2699–3702.

Keawprak N, Tu R, and Goto T (2009) Thermoelectricity of $CaIrO_3$ ceramics prepared by spark plasma sintering. *Journal of the Ceramic Society of Japan* 117: 466–469.

Keppler H, Dubrovinsky LS, Narygina O, and Kantor I (2008) Optical absorption and radiative thermal conductivity of silicate perovskite to 125 gigapascals. *Science* 322: 1529–1532. http://dx.doi.org/10.1126/science.1164609.

Kesson SE, Fitz Gerald JD, and Shelley JM (1998) Mineralogy and dynamics of a pyrolite lower mantle. *Nature* 393: 252–255.

Knittle E and Jeanloz R (1987) Synthesis and equation of state of (Mg, Fe)SiO_3 perovskite to over 100 GPa. *Science* 235: 668–670.

Kohn W and Sham LJ (1965) Self-consistent equations including exchange and correlation effects. *Physical Review* 140: A1133–A1138.

Kojitani H, Furukawa A, and Akaogi M (2007) Thermochemistry and high-pressure equilibria of the post-perovskite phase transition in $CaIrO_3$. *American Mineralogist* 92: 229–232.

Konishi K, Kawai K, Geller RJ, and Fuji N (2009) MORB in the lowermost mantle beneath the western Pacific: Evidence from waveform inversion. *Earth and Planetary Science Letters* 278: 219–225.

Labrosse S, Hernlund JW, and Coltice N (2007) A crystallizing dense magma ocean at the base of the Earth's mantle. *Nature* 450: 866–869.

Lay T (2008) Sharpness of the D″ discontinuity beneath the Cocos Plate: Implications for the perovskite to post-perovskite phase transition. *Geophysical Research Letters* 35: L03304. http://dx.doi.org/10.1029/2007GL032465.

Lay T and Garnero EJ (2004) Core–mantle boundary structures and processes. In: Sparks RSJ and Hawkesworth CJ (eds.) *The State of the Planet: Frontiers and Challenges in Geophysics*, pp. 25–42. Washington, DC: AGU.

Lay T and Garnero EJ (2013) Reconciling the post-perovskite phase with seismological observations of lowermost mantle structure. In: Hirose K, Brodholt J, Lay T, and Yuen D (eds.) *Post-Perovskite: The Last Mantle Phase Transition*. Washington, DC: American Geophysical Union, http://dx.doi.org/10.1029/174GM11.

Lay T, Garnero EJ, and Williams Q (2004) Partial melting in a thermo-chemical boundary layer at the base of the mantle. *Physics of the Earth and Planetary Interiors* 146: 441–467.

Lay T and Helmberger DV (1983) A lower mantle S-wave triplication and the velocity structure of D″. *Geophysical Journal of the Royal Astronomical Society* 75: 799–837.

Lay T, Hernlund J, and Buffett BA (2008) Core–mantle boundary heat flow. *Nature Geoscience* 1: 25–32.

Lay T, Hernlund J, Garnero EJ, and Thorne S (2006) A post-perovskite lens and D″ heat flux beneath the central Pacific. *Science* 314: 1272–1276.

Lay T, Williams Q, and Garnero E (1998) The core–mantle boundary layer and deep mantle dynamics. *Nature* 392: 461–468.

Lay T, Williams Q, Garnero EJ, Kellogg L, and Wysession MF (1998) Seismic wave anisotropy in the D″ region and its implications. In: Gurnis M, et al. (ed.) *The Core–Mantle Boundary Region*, pp. 299–318. Washington, DC: AGU.

Lay T and Young CJ (1989) Waveform complexity in teleseismic broadband SH displacements: Slab diffractions or deep mantle reflections? *Geophysical Research Letters* 16: 605–608.

Li J and Yuen DA (2014) Mid-mantle heterogeneities associated with Izanagi plate: Implications for regional mantle viscosity. *Earth and Planetary Science Letters* 385: 137–144.

Lin JF, Vankó G, Jacobsen SD, et al. (2007) Spin transition zone in Earth's lower mantle. *Science* 317: 1740–1743.

Lin JF, Weir ST, Jackson DD, et al. (2007) Electrical conductivity of the lower-mantle ferropericlase across the electronic spin transition. *Geophysical Research Letters* 34: L16305. http://dx.doi.org/10.1029/2007GL030523.

Liu L-G (1974) Silicate perovskite from phase transformation of pyrope-garnet at high pressure and temperature. *Geophysical Research Letters* 1: 277–280.

Manthilake GM, de Koker N, Frost DJ, and McCammon C (2011) Lattice thermal conductivity of lower mantle minerals and heat flux from Earth's core. *Proceedings of the National Academy of Sciences of the United States of America* 108: 17901–17904.

Mao WL, Meng Y, Shen G, et al. (2005) Iron-rich silicates in the Earth's D″ layer. *Proceedings of the National Academy of Sciences of the United States of America* 102: 9751–9753.

Mao WL, Shen G, Prakapenka VB, et al. (2004) Ferromagnesian postperovskite silicates in the D″ layer of the earth. *Proceedings of the National Academy of Sciences of the United States of America* 101: 15867–15869.

Marcy G and Butler RP (1995) Radial velocity surveys for Brown Dwarfs and planets. In: Tinney C (ed.) *The Bottom of the Main Sequence- and Beyond*, *Proceedings of the Workshop Held at ESO, Garching, Germany, 8–10 August 1994*, p. 98.

Martin CD, Crichton WA, Liu HZ, Prakapenka VB, Chen J, and Parise JB (2006) In-situ Rietveld structure refinement of perovskite and post-perovskite phases of $NaMgF_3$ (Neighborite) at high pressures. *American Mineralogist* 91(10): 1703–1706.

Marumo R and Syono Y (1971) *Acta Crystallographica* B27: 1868.

Maruyama S, Zhao D, and Santosh M (2007) Superplume, supercontinent, and post-perovskite: Mantle dynamics and anti-plate tectonics on the Core–Mantle Boundary. *Gondwana Research* 11: 7–37.

Masters G, Laske G, Bolton H, and Dziewonski A (2000) The relative behavior of shear velocity, bulk sound velocity, and compressional velocity in the mantle: Implications for chemical and thermal structure. In: Karato S, et al. (ed.) *Earth's Deep Interior*, pp. 63–88. Washington, DC: AGU.

Matsui M, Ito E, Katsura T, et al. (2009) The temperature–pressure–volume equation of state of platinum. *Journal of Applied Physics* 105: 013505.

Matyska C and Yuen DA (2005) The importance of radiative heat transfer on superplumes in the lower mantle with the new post-perovskite phase change. *Earth and Planetary Science Letters* 234: 71–81.

McCammon C, Kantor I, Narygina O, et al. (2008) Stable intermediate-spin ferrous iron in lower-mantle perovskite. *Nature Geoscience* 1: 684–687.

McDaniel CL and Schneider SJ (1972) Phase relation in the CaO–IrO_2–Ir system in air. *Journal of Solid State Chemistry* 4: 275–280.

McDonough WF and Sun SS (1995) The composition of the Earth. *Chemical Geology* 120: 223–253.

Merkel S, Kubo A, Miyagi L, et al. (2006) Plastic deformation of $MgGeO_3$ post-perovskite at lower mantle pressures. *Science* 311: 644–646.

Merkel S, McNamara AK, Kubo A, et al. (2007) Deformation of (Mg, Fe)SiO_3 post-perovskite and D″ anisotropy *Science* 316: 1729–1732. http://dx.doi.org/10.1126/science.1140609.

Miyagi L, Kanitpanyacharoen W, Kaercher P, Lee KKM, and Wenk HR (2010) Slip systems in $MgSiO_3$ post-perovskite: Implications for D″ anisotropy. *Science* 329: 1639–1642.

Miyajima N, Ohgushi K, Ichihara M, and Yagi T (2006) Crystal morphology and dislocation microstructures of $CaIrO_3$: A TEM study of an analogue of the $MgSiO_3$ post-perovskite phase. *Geophysical Research Letters* 33: L12302. http://dx.doi.org/10.1029/2005GL025001.

Monnereau M and Yuen DA (2007) Topology of the postperovskite phase transition and mantle dynamics. *Proceedings of the National Academy of Sciences of the United States of America* 104: 9156–9161.

Monnereau M and Yuen DA (2010) Seismic imaging of the D″ and constraints on the core heat flux. *Physics of the Earth and Planetary Interiors* 180: 258–270.

Morra G, Yuen DA, and Cammarano F (2010) Slabs and plumes crossing a broad density/viscosity discontinuity in the mid lower mantle. In: *AGU Abstract*, *Fall Meeting*.

Murakami M, Hirose K, Kawamura K, Sata N, and Ohishi Y (2004) Post-perovskite phase transition in $MgSiO_3$. *Science* 304: 855–858.

Murakami M, Hirose K, Sata N, and Ohishi Y (2005) Post-perovskite phase transition and crystal chemistry in the pyrolitic lowermost mantle. *Geophysical Research Letters* 32: L03304. http://dx.doi.org/10.1029/2004GL021956.

Murakami M, Ohishi Y, Hirao N, and Hrose K (2012) A perovskitic lower mantle inferred from high-pressure, high-temperature sound velocity data. *Nature* 485: 90–94.

Nakada M and Karato SI (2012) Low viscosity of the bottom of the Earth's mantle inferred from the analysis of Chandler wobble and tidal deformation. *Physics of the Earth and Planetary Interiors* 192–193: 68–80.

Nakagawa T and Tackley P (2004) Effects of a perovskite–post perovskite phase change mantle boundary in compressible mantle. *Geophysical Research Letters* 31: L16611. http://dx.doi.org/10.1029/2004GL020648.

Nakagawa T and Tackley PJ (2005) The interaction between the post-perovskite phase change and a thermo-chemical boundary layer near the core–mantle boundary. *Earth and Planetary Science Letters* 238: 204–216.

Nakagawa T and Tackley PJ (2006) Three-dimensional structures and dynamics in the deep mantle: Effects of post-perovskite phase change and deep mantle layering. *Geophysical Research Letters* 33: L21S11. http://dx.doi.org/10.1029/2005GC000967.

Nakagawa T and Tackley PJ (2011) Effects of low-viscosity post-perovskite on thermo-chemical mantle convection in a 3-D spherical shell. *Geophysical Research Letters* 38: L04309. http://dx.doi.org/10.1029/2010GL046494.

Nakagawa T, Tackley PJ, Deschamps F, and Connolly JAD (2012) Radial 1-D seismic structures in the deep mantle in mantle convection simulations with self-consistently calculated mineralogy. *Geochemistry, Geophysics, Geosystems* 13: Q11002. http://dx.doi.org/10.1029/2012GC004325.

Nakagawa T, Tackley PJ, Deschamps F, and Connoly JAD (2010) The influence of MORB and harzburgite composition on thermo-chemical mantle convection in a 3-D spherical shell with self-consistently calculated mineral physics. *Earth and Planetary Science Letters* 296: 403–412.

Nemeth P, Leinenweber K, Groy TL, and Buseck PR (2007) A new high pressure $CaGe_2O_5$ polymorph with 5- and 6-coordinated germanium. *American Mineralogist* 92: 441–443.

Nishihara Y, Aoiki I, Takahashi E, Matsukage KN, and Funakoshi K (2005) Thermal equation of stat of marjorite with MORB composition. *Physics of the Earth and Planetary Interiors* 148: 73–84. http://dx.doi.org/10.1016/j.pepi.2004.08.003.

Niwa K, Yagi T, Ohgushi K, Merkel S, Miyajima N, and Kikegawa T (2007) Lattice preferred orientation in $CaIrO_3$ perovskite and post-perovskite formed by plastic deformation under pressure. *Physics and Chemistry of Minerals*, in press.

Noel PH and Padiou J (1976) Structure cristalline de $FeUS_3$. *Acta Crystallographica* 32: 1593–1595.

Nomura R, Hirose K, Uesugi K, et al. (2014) Low core–mantle boundary temperature inferred from the solidus of pyrolite. *Science Express* http://dx.doi.org/10.1126/science.1248186.

Oganov A, Brodholt JP, and Price GD (2001) The elastic constants of $MgSiO_3$ perovskite at pressures and temperatures of the Earth's mantle. *Nature* 411: 934–937.

Oganov AR, Martonak R, Laio A, Raiteri P, and Parrinello M (2005) Anisotropy of Earth's D″ layer and stacking faults in the $MgSiO_3$ post-perovskite phase. *Nature* 438: 1142–1144.

Oganov AR and Ono S (2004) Theoretical and experimental evidence for a post-perovskite phase of $MgSiO_3$ in Earth's D″ layer. *Nature* 430: 445–448.

Oganov AR and Ono S (2005) The high pressure phase of alumina and implications for Earth's D″ layer. *Proceedings of the National Academy of Sciences of the United States of America* 102: 10828–10831.

Ohgushi K, Gotou H, Yagi T, Kiuchi Y, Sakai F, and Ueda U (2006) Metal-insulator transition in $Ca_{1-x}Na_xIrO_3$ with post-perovskite structure. *Physical Review B* 74: 241104.

Ohta K, Cohen R, Hirose K, Haule K, Shimizu K, and Ohishi Y (2012) Experimental and theoretical evidence for pressure-induced metallization in FeO with rocksalt-type structure. *Physical Review Letters* 108: 026403.

Ohta K, Hirose K, Ichiki M, Shimizu K, Sata N, and Ohishi Y (2010) Electrical conductivities of pyrolitic mantle and MORB materials up to the lowermost mantle conditions. *Earth and Planetary Science Letters* 289: 497–502. http://dx.doi.org/10.1016/j.epsl.2009.11.042.

Ohta K, Hirose K, Lay T, Sata N, and Ohishi Y (2006) The sharpness and compositional effects on post-perovskite phase transition. *Geochimica et Cosmochimica Acta* 70: A454.

Ohta K, Hirose K, Onoda S, and Shimizu K (2007) The effect of iron spin transition on electrical conductivity of (Mg, Fe)O magnesiowüstite. *Proceedings of the Japan Academy, Series B* 83: 97–100.

Ohta K, Hirose K, Shimizu K, Sata N, and Ohishi Y (2010) The electrical resistance measurements of (Mg, Fe)SiO_3 perovskite at high pressures and implications for electronic spin transition of iron. *Physics of the Earth and Planetary Interiors* 180: 154–158.

Ohta K, Hirose K, Lay T, Sata N, and Ohishi Y (2008a) Phase transitions in pyrolite and MORB at lowermost mantle conditions: Implications for a MORB-rich pile above the core-mantle boundary. *Earth and Planetary Science Letters* 267: 107–117.

Ohta K, Onoda S, Hirose K, et al. (2008b) The electrical conductivity of post-perovskite in Earth's D″ layer. *Science* 320: 89–91.

Ohta K, Yagi T, Taketoshi N, et al. (2012) Lattice thermal conductivity of $MgSiO_3$ perovskite and post-perovskite at the core–mantle boundary. *Earth and Planetary Science Letters* 349–350: 109–115.

Okada T, Yagi T, Niwa K, and Kikegawa T (2010) Lattice-preferred orientations in post-perovskite-type $MgGeO_3$ formed by transformations from different pre-phases. *Physics of the Earth and Planetary Interiors* 180: 195–202. http://dx.doi.org/10.1016/j.pepi.2009.08.002.

O'Neill C and Lenardic A (2007) Geological consequences of super-sized earths. *Geophysical Research Letters* 34(2007), L19204.

Ono S, Kikegawa T, and Ohishi Y (2004) High-pressure phase transition of hematite Fe_2O_3. *Journal of Physics and Chemistry of Solids* 65: 1527–1530.

Ono S and Oganov AR (2005) In situ observations of phase transition between perovskite and $CaIrO_3$-type phase in $MgSiO_3$ and pyrolitic mantle composition. *Earth and Planetary Science Letters* 236: 914–932.

Ono S, Oganov AR, Koyama T, and Shimizu H (2006) Stability and compressibility of the high-pressure phases of Al_2O_3 up to 200 GPa: Implications for the electrical conductivity of the base of the lower mantle. *Earth and Planetary Science Letters* 246: 326–335.

Ono S and Ohishi Y (2005) In situ X-ray observation of phase transformation in Fe_2O_3 at high pressures and high temperatures. *Journal of Physics and Chemistry of Solids* 66: 1714–1720.

Ono S, Ohishi Y, Isshiki M, and Watanuki T (2005) In situ X-ray observations of phase assemblages in peridotite and basalt compositions at lower mantle conditions: Implications for density of subducted oceanic plate. *Journal of Geophysical Research* 110: B02208. http://dx.doi.org/10.1029/2004JB003196.

Osako M and Ito E (1991) Thermal diffusivity of $MgSiO_3$ perovskite. *Geophysical Research Letters* 18: 239–242.

Panning M and Romanowicz B (2004) Inferences on flow at the base of Earth's mantle based on seismic anisotropy. *Science* 303: 351–353.

Perdew JP, Burke K, and Ernzerhof M (1996) Generalized gradient approximation made simple. *Physical Review Letters* 77: 3865–3868.

Perdew J and Zunger A (1981) Self-interaction correction to density functional approximations for many-electron systems. *Physical Review B* 23: 5048–5079.

Revenaugh J and Jordan TH (1991) Mantle layering from ScS reverberations. 4. The lower mantle and core–mantle boundary. *Journal of Geophysical Research* 96: 19811–19824.

Ricolleau A, Fei Y, Cottrell E, et al. (2009) Density profile of pyrolite under the lower mantle conditions. *Geophysical Research Letters* 36: L06302. http://dx.doi.org/10.1029/2008GL036759.

Ricolleau A, Perrillat JP, Fiquet G, et al. (2010) Phase relations and equation of state of a natural MORB: Implications for the density profile of subducted oceanic crust in the Earth's lower mantle. *Journal of Geophysical Research* 115: B08202. http://dx.doi.org/10.1029/2009JB006709.

Ringwood AE (1985) *Composition and Petrology of the Earth's Mantle*. McGraw-Hill International Series in the Earth and Planetary Sciences.

Romanowicz B (2001) Can we resolve 3D density heterogeneity in the lower mantle? *Geophysical Research Letters* 28: 1107–1110.

Samuel H and Tosi N (2012) The influence of post-perovskite strength on the Earth's mantle thermal and chemical evolution. *Earth and Planetary Science Letters* 323–324: 50–59. http://dx.doi.org/10.1016/j.epsl.2012.01.024.

Santillán J, Shim S-H, Shen G, and Prakapenka VB (2006) High-pressure phase transition in Mn_2O_3: Application for the crystal structure and preferred orientation of the $CaIrO_3$ type. *Geophysical Research Letters* 33: L15307. http://dx.doi.org/10.1029/2006GL026423.

Schott B, Yuen DA, and Braun A (2002) The influences of composition- and temperature-dependent rheology in thermal-chemical convection on entrainment of the D″-layer. *Physics of the Earth and Planetary Interiors* 29(1–2): 43–65.

Schubert G, Yuen DA, and Turcotte DL (1975) Role of phase transitions in a dynamic mantle. *Geophysical Journal International* 42: 705–735.

Seager S, Kuchner M, Hier-Majumdier CA, and Militzer B (2007) Mass–radius relationships for solid exoplanets. *The Astrophysical Journal* 669: 1279–1297.

Shim SH, Duffy TS, Jeanloz R, and Shen G (2004) Stability and crystal structure of $MgSiO_3$ perovskite to the core–mantle boundary. *Geophysical Research Letters* 31: L10603. http://dx.doi.org/10.1029/2004GL019639.

Sidorin I, Gurnis M, and Helmberger DV (1999) Evidence for a ubiquitous seismic discontinuity at the base of the mantle. *Science* 286: 1326–1329.

Sinmyo R and Hirose K (2010) The Soret diffusion in laser-heated diamond-anvil cell. *Physics of the Earth and Planetary Interiors* 180: 172.

Sinmyo R, Hirose K, Muto S, Ohishi Y, and Yasuhara A (2011) The valence state and partitioning of iron in the Earth's lowermost mantle. *Journal of Geophysical Research* 116: B07205. http://dx.doi.org/10.1029/2010JB008179.

Sotin C, Grasset O, and Mocquet A (2007) Mass-radio for extrasolar Earth-like planets and ocean planets. *Icarus* 191: 337–351.

Speziale S, Zha C, Duffy TS, Hemley RJ, and Mao HK (2001) Quasi-hydrostatic compression of magnesium oxide to 52 GPa: Implications for the pressure–volume–temperature equation of state. *Journal of Geophysical Research* 106: 515–528.

Stacey F (1992) *Physics of the Earth*, 3rd edn Brisbane, Australia: Brookfield.

Stacey FD and Loper DE (2007) A revised estimate of the conductivity of iron alloy at high pressure and implications for the core energy balance. *Physics of the Earth and Planetary Interiors* 161: 13–18.

Stackhouse S and Brodholt JP (2007) High-temperature elasticity of $MgSiO_3$ postperovskite. In: Hirose K, Brodholt JP, Lay T, and Yuen DA (eds.) *Post-*

Perovskite: The Last Mantle Phase Transition, pp. 99–113. Washington, DC: American Geophysical Union.

Stackhouse S, Brodholt JP, and Price GD (2005) High temperature elastic anisotropy of the perovskite and post-perovskite polymorphs of Al_2O_3. *Geophysical Research Letters* 32: L13305. http://dx.doi.org/10.1029/2005GL023163.

Stackhouse S, Brodholt JP, and Price GD (2006) Elastic anisotropy of $FeSiO_3$ end-members of the perovskite and post-perovskite phases. *Geophysical Research Letters* 33: L01304. http://dx.doi.org/10.1029/2005GL023887.

Stackhouse S, Brodholt J, and Price GD (2007) Electronic spin transitions in iron-bearing $MgSiO_3$ perovskite. *Earth and Planetary Science Letters* 253(1–2): 282–290. http://dx.doi.org/10.1016/j.epsl.2006.10.035.

Stackhouse S, Brodholt JP, Wookey J, Kendall J-M, and Price GD (2005) The effect of temperature on the seismic anisotropy of the perovskite and post-perovskite polymorphs of $MgSiO_3$. *Earth and Planetary Science Letters* 230: 1–10.

Stackhouse S, Stixrude L, and Karki BB (2010) Thermal conductivity of periclase (MgO) from first principles. *Physical Review Letters* 104: 208501.

Steinbach VC and Yuen DA (1994) Melting instabilities in the transition zone. *Earth and Planetary Science Letters* 127: 67–75.

Stixrude L (1997) Structure and sharpness of phase transitions and mantle discontinuities. *Journal of Geophysical Research* 102: 14835–14852. http://dx.doi.org/10.1029/97JB00550.

Tackley PJ, Amman M, Brodholt JP, Dobson DP, and Valencia D (2013) Mantle dynamics in Super-Earth: Post-perovskite rheology and self-regulation of viscosity. *Icarus* 225: 50–61.

Tackley PJ, Nakagawa T, and Hernlund JW (2007) Influence of the post-perovskite transition on thermal and thermo-chemical mantle convection. In: Hirose K, et al. (ed.) *Post-Perovskite: The Last Mantle Phase Transition*. *AGU Monograph*. Washington, DC: American Geophysical Union, http://dx.doi.org/10.1029/174GM11.

Tackley PJ, Stevenson DJ, Glatzmaier GA, and Schubert G (1993) Effects of an endothermic phase transition at 670 km depth in a spherical model of convection in the Earth's mantle. *Nature* 361: 699–705.

Tang X and Dong J (2010) Lattice thermal conductivity of MgO at conditions of Earth's interior. *Proceedings of the National Academy of Sciences of the United States of America* 107: 4539–4543.

Tateno S, Hirose K, Sata N, and Ohishi Y (2005) Phase relations in $Mg_3Al_2Si_3O_{12}$ to 180 GPa: Effect of Al on post-perovskite phase transition. *Geophysical Research Letters* 32: L15306. http://dx.doi.org/10.1029/2005GL023309.

Tateno S, Hirose K, Sata N, and Ohishi Y (2006) High-pressure behavior of $MnGeO_3$ and $CdGeO_3$ and the post-perovskite phase transition. *Physics and Chemistry of Minerals* 32: 721–725.

Tateno S, Hirose K, Sata N, and Ohishi Y (2007) High solubility of FeO in perovskite and the post-perovskite phase transition. *Physics of the Earth and Planetary Interiors* 160: 319–325.

Tateno S, Hirose K, Sata N, and Ohishi Y (2009) Determination of post-perovskite phase transition boundary up to 4,400 K and implications for thermal structure in D″ layer. *Earth and Planetary Science Letters* 277: 130–136.

Tolstikhin I and Hofmann AW (2005) Early crust on top of the Earth's core. *Physics of the Earth and Planetary Interiors* 148: 109–130.

Tosi N, Čadek O, Martinec Z, Yuen DA, and Kaufmann G (2009) Is the long-wavelength geoid sensitive to the presence of postperovskite above the core–mantle boundary? *Geophysical Research Letters* 36: L05303. http://dx.doi.org/10.1029/2008GL036902.

Tosi N, Yuen DA, and Čadek O (2010) Dynamical consequences in the lower mantle with the post-perovskite phase change and strongly depth-dependent thermodynamic and transport properties. *Earth and Planetary Science Letters* 298(229–243): 2010. http://dx.doi.org/10.1016/j.epsl.2010.

Tosi N, Yuen D, de Koker N, and Wentzcovitch RM (2013) Mantle dynamics with pressure- and temperature-dependent thermal expansivity and conductivity. *Physics of the Earth and Planetary Interiors* 217: 48–58. http://dx.doi.org/10.1016/j.pepi.2013.02.004.

Tozer DC (1972) The present thermal state of the terrestrial planets. *Physics of the Earth and Planetary Interiors* 6: 182–197.

Trampert J, Deschamps F, Resovsky J, and Yuen D (2004) Probabilistic tomography maps chemical heterogeneities throughout the lower mantle. *Science* 306: 853–856.

Tsuchiya T (2003) First-principles prediction of the *P–V–T* equation of state of gold and the 660-km discontinuity in Earth's mantle. *Journal of Geophysical Research* 108. http://dx.doi.org/10.1029/2003JB002446.

Tsuchiya J and Tsuchiya T (2008) Postperovskite phase equilibria in the $MgSiO_3$–Al_2O_3 system. *Proceedings of the National Academy of Sciences of the United States of America* 105: 19160–19164.

Tsuchiya T and Tsuchiya J (2011) Prediction of a hexagonal SiO_2 phase affecting stabilities of $MgSiO_3$ and $CaSiO_3$ at multimegabar pressures. *Proceedings of the National Academy of Sciences of the United States of America* 108: 1252–1255.

Tsuchiya T, Tsuchiya J, Umemoto K, and Wentzcovitch RM (2004a) Elasticity of post-perovskite $MgSiO_3$. *Geophysical Research Letters* 31: L14603. http://dx.doi.org/10.1029/2004GL020278.

Tsuchiya T, Tsuchiya J, Umemoto K, and Wentzcovitch RM (2004b) Phase transition in $MgSiO_3$ perovskite in the Earth's lower mantle. *Earth and Planetary Science Letters* 224: 241–248.

Tsuchiya J, Tsuchiya T, and Wentzcovitch RM (2005a) Vibrational and thermodynamic properties of $MgSiO_3$ post-perovskite. *Journal of Geophysical Research* 110(B2): B02204/1-6.

Tsuchiya J, Tsuchiya T, and Wentzcovitch RM (2005b) Transition from Rh_2O_3(II) to $CaIrO_3$-type structure and the high-pressure–temperature phase diagram of alumina. *Physical Review* B72: 020103.

Tsuchiya T, Wentzcovitch RM, da Silva CRS, and de Gironcoli S (2006) Spin transition in magnesiowüstite in Earth's lower mantle. *Physical Review Letters* 96: 198501.

Umemoto K, Hsu H, and Wentzcovitch RM (2010) Effect of site degeneracies on the spin crossovers in (Mg, Fe)SiO_3 perovskite. *Physics of the Earth and Planetary Interiors* 180: 209–214.

Umemoto K and Wentzcovitch RM (2011) Two-stage dissociation of $MgSiO_3$ post-perovskite. *Earth and Planetary Science Letters* 311: 225.

Umemoto K, Wentzcovitch RM, and Allen PB (2006) Dissociation of $MgSiO_3$ in the cores of gas giants and terrestrial exoplanets. *Science* 311: 983–985.

Umemoto K, Wentzcovitch RM, Parise J, and Weidner D (2006) $NaMgF_3$: A low pressure analog of $MgSiO_3$. *Geophysical Research Letters* 33: L15304.

Valencia D, O'Connell RJ, and Sasselov D (2006) Internal structure of massive terrestrial planets. *Icarus* 181: 545–554.

Valencia D, O'Connell RJ, and Sasselov D (2007) Inevitability of plate tectonics in super-Earths. *The Astrophysical Journal* 670: L45–L48.

Valencia D, Sasselov D, and O'Connell RJ (2007a) Radius and structure model of the first Super-Earth planet. *The Astrophysical Journal* 565: 545–551.

Valencia D, Sasselov D, and O'Connell RJ (2007b) Detailed models of Super-Earths: How well can we infer bulk properties. *The Astrophysical Journal* 665: 1413–1420.

van den Berg AP, de Hoop MV, Yuen DA, Duchkov A, van der Hilst RD, and Jacobs MHG (2010a) Geodynamical modeling and multiscale seismic expression of thermo-chemical heterogeneity and phase transitions in the lowermost mantle. *Physics of the Earth and Planetary Interiors* 180: 244–257.

van den Berg A, Yuen DA, Beebe GL, and Christiansen MD (2010b) The dynamical impact of electronic thermal conductivity on deep mantle convection of exosolar planets. *Physics of the Earth and Planetary Interiors* 178: 136–154.

van der Hilst RD, de Hoop MV, Wang P, Shim SH, Ma P, and Tenoria L (2007) Seismostratigraphy and thermal structure of Earth's core–mantle boundary region. *Science* 315: 1813–1817.

van der Meer DG, Spakman W, van Hinsbergen DJJ, Amaru M, and Torsvik TH (2010) Towards absolute plate motions constrained by lower-mantle slab remnants. *Nature Geoscience* 3: 36–40.

Wallace D (1972) *Thermodynamics of Crystals*. New York: Wiley.

Walte N, Heidelbach F, Miyajima N, and Frost D (2007) Texture development and TEM analysis of deformed $CaIrO_3$: Implications for the D″ layer at the core–mantle boundary. *Geophysical Research Letters* 34: L08306. http://dx.doi.org/10.1029/2007GL029407.

Walte NP, Heidelbach F, Miyajima N, Frost DJ, Rubie DC, and Dobson DP (2009) Transformation textures in post-perovskite: Understanding mantle flow in the D″ layer of the Earth. *Geophysical Research Letters* 36: L04302. http://dx.doi.org/10.1029/2008GL036840.

Wang P, de Hoop MV, van der Hilst RD, Ma P, and Tenorio L (2006) Imaging of structure at and near the core–mantle boundary using a generalized Radon transform. 1. Construction of image gatherers. *Journal of Geophysical Research* 111(B12): B1230.

Weber M, Davis JP, Thomas C, et al. (1996) The structure of the lowermost mantle as determined from using seismic arrays. In: Boschi E, Ekstrom G, and Morelli A (eds.) *Seismic Modeling of the Earth's Structure*, pp. 399–442. Rome: Istit. Naz. di Geophys.

Weinstein SA (1995) The effects of a deep mantle endothermic phase change on the structure of thermal convection in silicate planets. *Journal of Geophysical Research* 100(E6): 1171911728.

Wentzcovitch RM, Justo JF, Wu Z, da Silva CRS, Yuen D, and Kohlstedt D (2009) Anomalous compressibility of ferropericlase throughout the iron spin crossover. *Proceedings of the National Academy of Sciences of the United States of America* 106: 8447–8452.

Wentzcovitch RM, Karki BB, Cococcioni M, and de Gironcoli S (2004) Thermoelastic properties of $MgSiO_3$-perovskite: Insights on the nature of the Earth's lower mantle. *Physical Review Letters* 92: 018501.

Wentzcovitch RM, Martins JL, and Price GD (1993) Ab initio molecular dynamics with variable cell shape: Application to $MgSiO_3$. *Physical Review Letters* 70: 3947–3951.

Wentzcovitch RM, Ross N, and Price GD (1995) Ab initio investigation of $MgSiO_3$ and $CaSiO_3$-perovskites at lower mantle pressures. *Physics of the Earth and Planetary Interiors* 90: 101–112.

Wentzcovitch RM, Tsuchiya T, and Tsuchiya J (2006) $MgSiO_3$ post-perovskite at D″ conditions. *Proceedings of the National Academy of Sciences of the United States of America* 103: 543–546.

Wentzcovitch RM, Yu Y, and Wu Z (2010) Thermodynamic properties and phase relations in mantle minerals investigated by first principles quasiharmonic theory. *Reviews in Mineralogy & Geochemistry* 71: 59–98.

Wood BJ (2000) Phase transformations and partitioning relations in peridotite under lower mantle conditions. *Earth and Planetary Science Letters* 174: 341–354.

Wookey J, Stackhouse S, Kendall J-M, Brodholt J, and Price GD (2005) Efficacy of the post-perovskite phase as an explanation for lowermost-mantle seismic properties. *Nature* 438: 1004–1007.

Wu S, Ji M, Wang C-Z, et al. (2014) Adaptive genetic algorithm for crystal structure prediction. *Journal of Physics: Condensed Matter* 26: 035402. http://dx.doi.org/10.1088/0953-8984/26/3/035402.

Wu Z, Justo JF, and Wentzcovitch R (2013) Elastic anomalies in a spin-crossover system: Ferropericlase at lower mantle conditions. *Physical Review Letters* 110: 228501.

Wu S, Umemoto K, Ji M, Wang C-Z, Ho K-M, and Wentzcovitch RM (2011) Identification of post-pyrite phase transition in SiO_2 by genetic algorithm. *Physical Review B* 83: 184102.

Wu Z and Wentzovitch R (2013) *Lateral velocity variations of ferropericlase in Earth's lower mantle*. American Geophysical Union, Fall Meeting, abstract #DI51A-2278.

Wu Z and Wentzcovitch R (2014) Spin crossover in ferropericlase and lateral variations in the Earth's lower mantle, submitted for publication.

Wu Z, Wentzcovitch RM, Umemoto K, Li B, and Hirose K (2008) *P–V–T* relations in MgO: An ultra-high *P–T* scale for planetary sciences applications. *Journal of Geophysical Research* 113: B06204, Erratum in *J. Geophys. Res*. 115, B05201, 2010.

Wysession ME, Lay T, Revenaugh J, et al. (1998) The D″ discontinuity and its implications In: Gurnis M, et al. (ed.) *The Core–Mantle Boundary Region*, pp. 273–297. Washington, DC: AGU.

Xu W, Lithgow-Bertelloni C, Stixrude L, and Ritsema J (2008) The effect of bulk composition and temperature on mantle seismic structure. *Earth and Planetary Science Letters* 275: 70–79.

Xu Y, Shankland TJ, and Poe BT (2000) Laboratory-based electrical conductivity in the Earth's mantle. *Journal of Geophysical Research* 105: 27865–27875.

Yagi T (2007) Review of experimental studies on mantle phase transitions. In: Hirose K, Brodholt J, Lay T, and Yuen DA (eds.) *Post-Perovskite: The Last Mantle Phase Transition*, *Geophysics Monograph Series*, 174, pp. 9–18.

Yagi T, Ohta K, Kobayashi K, Taketoshi N, Hirose K, and Baba T (2011) Thermal diffusivity measurement in a diamond anvil cell using a light pulse thermo-reflectance technique. *Measurement Science and Technology* 22: 024011.

Yamazaki D and Karato S-I (2002) Fabric development in (Mg, Fe)O during large strain, shear deformation: Implications for seismic anisotropy in Earth's lower mantle. *Physics of the Earth and Planetary Interiors* 131: 251–267.

Yamazaki D, Yoshino T, Matsuzaki T, Katsura T, and Yoneda A (2009) Texture of (Mg, Fe)SiO_3 perovskite and ferro-periclase aggregate: Implications for rheology of the lower mantle. *Physics of the Earth and Planetary Interiors* 174: 138–144.

Yoshino T and Yamazaki D (2007) Grain growth kinetics of $CaIrO_3$ perovskite and post-perovskite, with implications for rheology of D" layer. *Earth and Planetary Science Letters* 255: 485–493.

Yuen DA, Monnereau M, Hansen U, Kameyama MC, and Matyska C (2007) Dynamics of superplumes in the lower mantle. In: Yuen DA, Maruyama S, Karato S, and Windley B (eds.) *Superplumes: Beyond Plate Tectonics*. Springer, Chapter 9.

Yuen DA and Peltier WR (1980) Mantle plumes and thermal stability of the D″ layer. *Geophysical Research Letters* 7: 625–628.

Yusa H, Sata N, Akaogi M, Kojitani H, Yamamoto R, and Ohishi Y (2005) High *P–T* transition in $ZnGeO_3$ up to 100 GPa. *Review of High Pressure Science and Technology* 15: 209.

Zhang F and Oganov AR (2006) Valence state and spin transitions of iron in Earth's mantle silicates. *Earth and Planetary Science Letters* 249(3–4): 436–443. http://dx.doi.org/10.1016/j.epsl.2006.07.023.

Zhang Z, Stixrude L, and Brodholt J (2013) Elastic properties of $MgSiO_3$-perovskite under lower mantle conditions and the composition of the deep Earth. *Earth and Planetary Science Letters* 370: 1–12.

Zhang D-B, Sun T, and Wentzcovitch RM (2014) Phonon quasi-particles and anharmonic free energy in complex systems. *Physical Review Letters* 115: 058501.